Efficient Displacement of Heavy Oil by Use of Three Hydrocarbon Phases

R. Okuno, SPE, and **Z. Xu,** SPE, University of Alberta

Summary

Mixtures of oil with solvent gas can exhibit three-hydrocarbon-phase behavior at reservoir conditions, where the solvent-rich liquid (L_2) phase coexists with the gaseous (V) and oleic (L_1) phases. Three-hydrocarbon-phase behavior has been studied in the literature for carbon dioxide (CO_2) floods and enriched-gas floods at relatively low temperatures. Prior research on heavy-oil displacement with enriched gas presented that displacement efficiency at a given throughput can be nonmonotonic with respect to gas enrichment. Slimtube experiments for such displacements showed that oil recovery increased first, then decreased, and increased again with increasing gas enrichment. An optimum displacement with a high efficiency of more than 90% was observed when three-hydrocarbon-phase flow was present. However, detailed mechanisms for such an optimum displacement with three phases have not been explained in the literature.

In this research, we investigate mass transfer on multiphase transitions between two and three phases for three-hydrocarbon-phase displacements. Simple conditions are derived for the multiphase transitions that yield high local displacement efficiency by three hydrocarbon phases. The derivation is based on the generalized mass conservation for a multiphase transition in 1D gas injection. The conditions derived are applied to explain nonmonotonic oil recovery in quaternary displacements and the West Sak oil displacements.

Oil recovery at a given throughput can be nonmonotonic with respect to pressure or gas enrichment. Such a nonmonotonic trend can occur when local oil displacement by three hydrocarbon phases becomes more efficient, but slower, with decreasing pressure or decreasing gas enrichment. An optimum pressure or enrichment can occur as a consequence of the balance between the local displacement efficiency and the propagation rate of three hydrocarbon phases. The West Sak oil displacement with enriched gas studied in this research yields a high displacement efficiency of more than 90% at 1.5 hydrocarbon pore volumes (PV) injected at 53% methane (C_1) dilution.

Introduction

Solvent injection is a widely used method for enhanced oil recovery (EOR) (Lake 1989; Taber et al. 1997; Orr 2007). Its implementation has been made for a wide variety of oil reservoirs: in West Texas (Mizenko 1992; Stein et al. 1992; Tanner et al. 1992), in Alaska (McGuire et al. 2001), in Canada (Malik and Islam 2000), and in the North Sea (Varotsis et al. 1986). Coinjection of steam and solvent could further widen the applicability of solvent to extraheavy oil and bitumen reservoirs. A few pilot tests for the coinjection were reported in the literature (Gupta et al. 2005; Gupta and Gittins 2006; Dickson et al. 2011).

Reliable design of solvent injection requires detailed understanding of oil-displacement mechanisms. Displacement theory for solvent injection has been established for conventional two-hydrocarbon phases (Orr 2007). Multicontact miscibility (MCM) between two phases can be developed through vaporizing, condensing, or combined condensing/vaporizing mechanisms (Dindoruk 1992; Johns 1992). An important design parameter for solvent injection is the thermodynamic minimum miscibility pressure (MMP). The thermodynamic MMP is the minimum displacement pressure at which complete miscibility is developed along a composition path from the injection-gas composition to the reservoir-oil composition for 1D flow in the absence of dispersion. Efficient methods have been developed for MMP calculation, where phase behavior and flow are effectively decoupled (Johns and Orr 1996; Ahmadi and Johns 2011).

Solvent injection is often conducted at partially miscible (PM) (or immiscible) conditions because it can be costly and difficult to achieve MCM conditions in situ, especially in a heavy-oil reservoir. Also, many solvent/oil mixtures can exhibit three hydrocarbon phases with partial miscibility at reservoir conditions (Gardner et al. 1981; Khan et al. 1992; Creek and Sheffield 1993). These are the oleic (L_1), solvent-rich liquid (L_2), and gaseous (V) phases. The three-hydrocarbon-phase behavior is characteristic of highly size-asymmetric mixtures as observed for n-alkane binaries and CO_2-n-alkane binaries (Rowlinson 1959; Polishuk et al. 2004). As summarized by Peters (1994), three-phase behavior bounded by two critical endpoints (CEPs) has been observed for n-alkane binaries; C_1/nC_6, C_1/nC_7, C_2/n-alkanes from nC_{18} through nC_{25}; and C_3/n-alkanes heavier than nC_{30}. A CEP is a critical state where two of the three equilibrium phases become critical (Uzunov 1993). There are two types of CEPs: lower CEP (LCEP), where the L_1 and L_2 phases merge in the presence of the V phase ($L_1 = L_2 - V$), and upper CEP (UCEP), where the V and L_2 phases merge in the presence of the L_1 phase ($L_1 - L_2 = V$). In the abbreviated symbolic notation, the critical and noncritical equilibrium states are expressed by use of "=" and "–", respectively.

Modeling of the complex three-phase behavior has been also conducted by use of various equations of state (EOSs): the van der Waals EOS (van Konynenburg 1968; Scott and van Konynenburg 1970; van Konynenburg and Scott 1980; Bluma and Deiters 1999), the Redlich-Kwong EOS (Deiters and Schneider 1976; Deiters and Pegg 1989), the Peng-Robinson EOS (Gauter 1999; Gauter et al. 1999; Mushrif 2004; Yang 2006; Mushrif and Phoenix 2008), and the Soave-Redlich-Kwong EOS (Gregorowicz and de Loos 1996). The results show that a cubic EOS is capable of predicting three-phase behavior (van Konynenburg 1968).

There are major heavy-oil reservoirs on the North Slope of Alaska, such as the West Sak, Schrader Bluff, and Kuparuk oil reservoirs. The primary recovery and waterflooding were relatively inefficient in these heavy-oil reservoirs mainly because of high oil viscosity. Solvent injection has been studied because Prudhoe Bay artificial-lift gas and Prudhoe Bay natural-gas liquid are both available as solvent (Sharma et al. 1989; Hornbrook et al. 1991; DeRuiter et al. 1994; Godbole et al. 1995; Khataniar et al. 1999; McKean et al. 1999; Wang and Strycker 2000; Madarapu et al. 2002; Li et al. 2003; Wang et al. 2003; McGuire et al. 2005; Targac et al. 2005; Aghbash and Ahmadi 2012). Conventional thermal methods were considered to be impractical because of high well costs, large well spacing, and thick permafrost (McGuire et al. 2005).

Mixtures of heavy oil and solvent exhibit complex multiphase behavior at low reservoir temperature (50–100°F) because of proximity to the permafrost in the region (DeRuiter et al. 1994). A number of authors presented experimental phase-behavior studies for these heavy oils: the West Sak oil (Shu and Hartman 1988; Roper 1989; Sharma et al. 1989; Hornbrook et al. 1991; Okuyiga 1992; DeRuiter et al. 1994; Mohanty et al. 1995; McGuire et al.

This paper (SPE 165470) was accepted for presentation at the SPE Heavy Oil Conference Canada, Calgary, 11–13 June 2013, and revised for publication. Original manuscript received for review 29 March 2013. Revised manuscript received for review 6 December 2013. Paper peer approved 17 January 2014.

2005), the Schrader Bluff oil (Inaganti 1994; Reid 1994; Khataniar et al. 1999; McKean et al. 1999; Wang and Strycker 2000; Madarapu et al. 2002), and the Kuparuk oil (Godbole et al. 1995). Multiphase behavior involving the L_1, L_2, and V phases was observed in their static experiments and slimtube tests.

Various numerical-simulation studies were also conducted with concerns about sweep efficiency, which is typically low for gas injection in a viscous oil reservoir because of gravity segregation; front instability; and heterogeneity (Mohanty et al. 1995; Guler et al. 2001; Madarapu et al. 2002; Li et al. 2003; Wang et al. 2003; Sohrabi et al. 2007). Most of the studies considered water-alternating-gas (WAG) injection. In numerical simulations by Guler et al. (2001) and Wang et al. (2003), oil displacement by the L_2 phase exhibited less gravity segregation than expected from conventional oil displacement by gas. This was because the liquid-like density of the L_2 phase at the reservoir conditions made the density difference between the L_1 and L_2 phases less significant. Also, the formation of multiple liquid phases during the displacements was found to make displacement fronts less unstable (Mohanty et al. 1995; Sohrabi et al. 2007). This was consistent with experimental observations by DeRuiter et al. (1994) and Khataniar et al. (1999).

The in-situ formation of multiple liquid phases was observed to decrease the total mobility of the transition zone in gas displacements (Henry and Metcalfe 1983). The reduced injectivity observed in the North Cross Devonian CO_2 flood was partially attributed to the formation of three hydrocarbon phases (Pontious and Tham 1978). Patel et al. (1987) concluded that phase behavior does not necessarily create injectivity decreases by itself. Rogers and Grigg (2001) stated that there is no clear experimental evidence that multiphase behavior effects result in field-observed fluid mobilities. Targac et al. (2005) described that the injectivity in West Sak has been substantially increased with the evolution in horizontal and multilateral drilling technology. Guler et al. (2001) stated that the presence of initial mobile water in the Schrader Bluff oil reservoir could increase the solvent injectivity. An extensive literature analysis on injectivity behavior in various CO_2 floods can be found in Rogers and Grigg (2001).

A large three-hydrocarbon-phase region was observed during slimtube experiments in DeRuiter et al. (1994) and Mohanty et al. (1995). Mohanty et al. (1995) also confirmed three-hydrocarbon-phase flow in 1D numerical simulations by use of the UTCOMP simulator (Chang et al. 1990). The UTCOMP simulator is an EOS compositional multiphase reservoir simulator developed at the University of Texas at Austin. It is based on the implicit-pressure/explicit-concentration (IMPEC) formulation. However, coexistence of the three hydrocarbon phases was much less obvious in multidimensional simulations of solvent injection for Alaskan heavy oils in Guler et al. (2001) and Madarapu et al. (2002). These results indicate that gravity, channeling, and dispersion affect compositional propagation in the multidimensional multiphase flow.

Chang et al. (1994) and Chang (1990) presented a systematic investigation of reservoir-flow patterns in CO_2 floods, such as viscous fingering, channeling, gravity override, and dispersive flow. Multidimensional numerical simulations of CO_2 floods were conducted by use of the UTCOMP simulator with a wide range of endpoint mobility ratio, gravity number, effective aspect ratio, longitudinal- and transverse-Péclet number, correlation length, and Dykstra-Parsons coefficient. They showed that viscous fingering was unlikely as a dominant-flow pattern for field-scale CO_2 flooding under secondary conditions without use of WAG injection, which would reduce the tendency of fingering. They concluded that fingering should be taken into account under typical laboratory conditions of low effective aspect ratio and low permeability variation, but fingering would be much less likely to be important under reservoir conditions of high effective aspect ratio. The dominant flow patterns were channeling, gravity override, and dispersive flow for most of the cases studied. The fluid model used was a ternary model of a Maljamar separator oil given by Ogino (1988). Three hydrocarbon phases were not predicted with this ternary fluid, as presented in Chang (1990). The investigation by Tchelepi and Orr (1994) also suggested that channeling and gravity override would be dominant flow patterns if the reservoir was highly heterogeneous with large correlation lengths. To our knowledge, however, similar investigation of reservoir flow patterns with three hydrocarbon phases has not been presented in the literature. This is likely because of complex effects of three-hydrocarbon-phase behavior on oil recovery and various difficulties associated with three-phase behavior calculations in compositional simulation.

Heavy-oil displacement by three hydrocarbon phases is difficult to interpret even for 1D flow with no gravity (DeRuiter et al. 1994), which is the main focus of this paper. Prior studies showed that 1D oil displacement with three hydrocarbon phases can exhibit displacement efficiency that is nonmonotonic with respect to gas enrichment at a given throughput. DeRuiter et al. (1994) and Mohanty et al. (1995) conducted slimtube experiments for the West Sak oil with enriched gas. Their results showed that oil recovery at 1.2 PV injected (PVI) first decreased, then increased, and finally decreased again with decreasing gas enrichment. Oil recoveries at 1.2 PVI were 97, 87, 89, 93 and 65% at 32-, 42-, 51-, 62-, and 70%-C_1 dilution, respectively. A maximum of 93% at 62%-C_1 dilution was substantially higher than 87% at a lower C_1 dilution of 42%.

DeRuiter et al. (1994) speculated that the nonmonotonic trend was associated with the coexistence of three hydrocarbon phases and their effects on the front mobility. The improvement in mobility ratio can improve sweep efficiency in multidimensional floods (Mohanty et al. 1995). However, the effect of miscibility (i.e., compositional phase behavior) would dominate over the fractional-flow effect in terms of local displacement efficiency in this PM flow with significant mass transfer among phases. Mohanty et al. (1995) later explained that oil recovery at 1.2 PVI was higher at 62%-C_1 dilution than at 51%-C_1 dilution because the L_2 phase was nearly miscible with the L_1 phase at the three-phase displacement front; oil became less viscous at the front; and the front moved fast enough to exit the slimtube by 1.2 PVI. No detailed theoretical explanation has been given in the literature as to what causes gas enrichment to decrease oil recovery.

The existing theory of gas injection does not explain a nonmonotonic trend of PM displacement efficiency. The length of the shortest tie-line monotonically decreases as pressure or gas enrichment increases in the conventional two-phase displacement when the fluid is properly characterized (Ahmadi 2011). Thus, the efficiency of the conventional two-phase displacement tends to increase monotonically until MCM is approached. A question then arises as to why the efficiency of three-hydrocarbon-phase displacement can decrease as gas enrichment (or displacement pressure) increases. We present in this paper that the reason is associated with multiphase transitions between two and three phases in three-phase PM displacements. The main novelty of this research is that simple conditions are developed for the mass transfer on multiphase transitions that yield high local displacement efficiency by three PM phases. Because of the complex phase behavior, the focus of this paper is on 1D oil displacement with no gravity. Decoupling of local-oil displacement from the effects of reservoir-flow patterns enables us to analyze detailed mass-transfer mechanisms during the complex multiphase displacements.

In the subsequent sections, we first discuss multiphase behavior in solvent injection by use of a synthetic quaternary system, which exhibits a decreasing trend of oil recovery with increasing displacement pressure or solvent enrichment. We then present a theoretical analysis of phase transitions in three-hydrocarbon-phase displacement. Conditions are derived for efficient oil displacement by three hydrocarbon phases, and are explained in detail by use of simulation cases with the quaternary system. Finally, the efficiency conditions are confirmed in fine-scale simulations for enriched-gas injection for the West Sak oil.

Characteristics of Oil Displacement With Three Hydrocarbon Phases

This section describes general characteristics of three-hydrocarbon-phase displacement in terms of multiphase transitions and their effects on displacement efficiency. The main difference

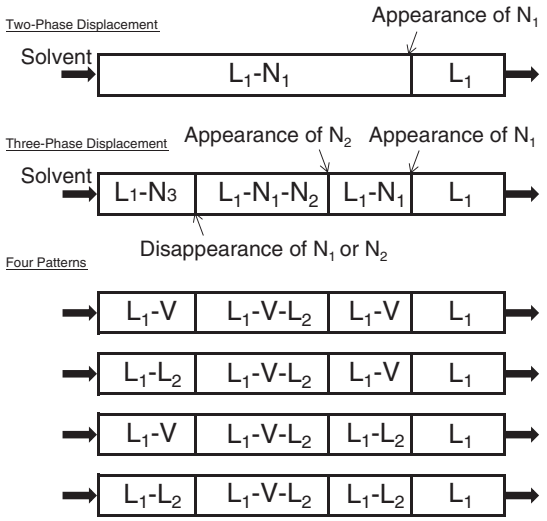

Fig. 1—Schematics of phase behavior in two- and three-phase displacements. The oleic phase is given as L_1. A nonoleic phase (N_1) appears at the displacement front for two- and three-phase displacements. For a three-phase displacement, another nonoleic phase (N_2) appears at the leading edge of the three-phase region. One of the two nonoleic phases (N_1 and N_2) in the three-phase region disappears at the trailing edge of the three-phase region. The nonoleic phase (N_3) in the upstream two-phase region is either N_1 or N_2, depending on the phase behavior involved there. Four possible patterns for three-phase displacement are also presented.

between two- and three-phase displacements is that the latter involves multiphase transitions between two and three phases. **Fig. 1** schematically shows phase behavior during two- and three-phase displacements. A two-phase displacement involves the L_1 phase and a nonoleic (N_1) phase. Although the N_1 phase is often the V phase in typical gasfloods, we do not specify its phase identity in the schematic, for generality. A phase transition between one and two phases occurs at the displacement front, where the N_1 phase appears. Complete evaporation of the L_1 phase is invisible in the schematic because the evaporation wave is normally much slower than the displacement front, especially in the presence of dispersion.

Phase behavior for three-phase displacement of oil is more involved. Two nonoleic phases appear in sequence in the direction from the producer to the injector. The nonoleic phase that appears first at the displacement front is referred to as N_1. The N_2 phase then appears at the leading edge of the three-phase region, which is at equilibrium with the L_1 and N_1 phases in the three-phase region. One of the two nonoleic phases disappears at the trailing edge of the three-phase region. The nonoleic phase that coexists with the L_1 phase in the upstream two-phase region is referred to as N_3, which is either N_1 or N_2 depending on the phase transition there.

There are four patterns for phase transitions for the three-phase displacement in Fig. 1 because the N_1/N_3 pair can be either V/V, or V/L_2, or L_2/V, or L_2/L_2. That is, the four patterns for (N_1, N_2, N_3) are as follows: (V, L_2, V), (V, L_2, L_2), (L_2, V, V), and (L_2, V, L_2). The two phases at the displacement front are typically the V and L_1 phases because of a fast-traveling C_1 bank. For the two phases upstream of the three-phase region, however, both L_1/V and L_1/L_2 are common depending on phase behavior near the injection-gas composition at the operating temperature and pressure. Although it is possible to have a direct transition between one phase and three phases without involving two-phase equilibrium, as shown in LaForce and Johns (2005a), we do not consider this type of phase transition in this research.

Existence of three phases during oil displacement with solvent indicates that the composition path goes through part of a three-phase region in composition space at the temperature and pressure. The entire three-phase region is not necessarily realized along the composition path. Thus, the three-phase behavior encountered during the displacement is considered as part of the entire three-phase region. The entire three-phase region can be considered to be bounded by two CEP behaviors in composition space (Okuno 2009; Okuno et al. 2011), as illustrated in Appendix A. A CEP is a critical phase behavior in which two of the three phases merge in the presence of the other immiscible phase. The L_1 and L_2 phases merge in the presence of the V phase at the LCEP, whereas the L_2 and V phases merge in the presence of the L_1 phase at the UCEP. Three-phase behavior bounded by the two types of CEPs is well-documented in the literature especially for n-alkane binaries (Rowlinson and Freeman 1961; Kohn et al. 1966) and CO_2/n-alkane binaries (Enick et al. 1985; Galindo and Blas 2002). Note that there are two equilibrium phases at a CEP; i.e., it is a tie-line rather than a point in composition space. In this paper, a CEP is sometimes called a CEP tie-line to avoid potential confusion.

Okuno et al. (2011) studied mechanisms of three-phase displacement of conventional oil with CO_2 solvent. Most of the phase transitions in their study were as follows: V for N_1, L_2 for N_2, and V for N_3. They used four components to conduct a systematic investigation of oil-displacement mechanisms involving three phases bounded by the UCEP and LCEP tie-lines. Results showed that high displacement efficiency of more than 90% at 2.0 hydrocarbon PVI (HCPVI) could be achieved when the composition path traversed near the UCEP and LCEP tie-lines. Oil components were efficiently extracted by the L_2 phase because of near-LCEP behavior at the leading edge of three phases. Near-UCEP behavior at the trailing edge of three phases then allowed the L_2 phase to efficiently merge into the V phase. That is, the L_2 phase served as a buffer between the immiscible V and L_1 phases within the three-phase region. They also confirmed this displacement mechanism for multicomponent systems based on west Texas oils. Although nearly piston-like displacements were simulated with three phases bounded by the CEP tie-lines, it was uncertain whether MCM could be developed through the CEP behavior.

Recent research on analytical solutions for three-phase displacements has significantly improved our understanding of miscibility development in three-phase flow (LaForce and Johns 2005b; LaForce et al. 2008a, 2008b; LaForce and Orr 2008, 2009; LaForce 2012). These studies considered analytical composition paths and miscibility development in water and gas injection by use of three and four components on the basis of the method of characteristics (MOC). The four components consisted of water, CO_2, and two hydrocarbon components. The quaternary cases with miscible-gas/water injection presented a CEP in composition space, at which the two hydrocarbon phases were critical in the presence of the aqueous (W) phase (i.e., a CEP of type $L_1 = V - W$). This was the only CEP in composition space in their research because the W phase was immiscible with the hydrocarbon phases. Their results indicated that MCM could be developed not only at the two-phase critical point ($L_1 = V$), but also on the CEP tie-line ($L_1 = V - W$). In such a case, the initial oil in the L/W region was completely displaced by CO_2 in the V/W region through the CEP tie-line. For complex three-hydrocarbon-phase flow with critical endpoints, however, analytical solutions by use of the MOC have not been presented in the literature, to the best of our knowledge.

Nonmonotonic Oil Recovery by Use of a Quaternary System

This section describes nonmonotonic oil recovery by use of a quaternary fluid, which is modeled after the Schrader Bluff oil model in Guler et al. (2001). Fine-scale compositional simulations are performed for linear oil displacement with no gravity. The UTCOMP simulator (Chang et al. 1990) with the Peng-Robinson EOS (Peng and Robinson 1976) is used for all flow simulations in this research. The UTCOMP simulator has been used in various papers on gas-injection theory (Mohanty et al. 1995; Johns et al. 2000, 2004; Solano et al. 2001). Because of numerical dispersion, the numerical-simulation results deviate from the analytical

TABLE 1—PROPERTIES OF THE QUATERNARY FLUID

	Oil (mol%)	Gas (mol%)	Molecular Weight	T_c (°R)	P_c (psia)	Acentric Factor	V_c (ft^3/lbm-mol)
PC1	37.22	20	17.268	357.77	666.48	0.0193	1.6763
PC2	10.63	80	40.288	630.32	656.22	0.1402	2.9740
PC3	30.11	0	352.25	1318.1	240.31	0.5574	21.572
PC4	22.04	0	1052.0	1967.3	94.80	1.1313	83.571

TABLE 2—BINARY INTERACTION PARAMETERS FOR THE QUATERNARY FLUID

Components	PC1	PC2	PC3	PC4
PC1	0	—	—	—
PC2	0.0052	0	—	—
PC3	0	0.0050	0	—
PC4	0.1822	0.1336	0	0

solutions based on the MOC for 1D gas injection. The deviation diminishes as the Péclet number becomes higher with more gridblocks. Recently, van Odyck et al. (2012) and Mallison et al. (2005) developed methods for accurately simulating displacement processes.

The four components consist of one light pseudocomponent (PC1), one intermediate pseudocomponent (PC2), and two heavy pseudocomponents (PC3 and PC4). Their properties are given in **Tables 1 and 2.** The oil gravity is calculated to be approximately 10°API. The injection gas consists of 20% PC1 and 80% PC2.

Fig. 2 shows the pressure/temperature (P/T) diagrams calculated for the quaternary oil and injection gas by use of PVTsim software (Calsep 2012). The bubblepoint pressure at the reservoir temperature of 86°F is 1,953 psia for the oil. The bubble- and dewpoint pressures at 86°F are 658 psia and 334 psia, respectively, for the injection gas. The critical point of the injection gas is calculated to be 144.88°F and 836.38 psia. **Fig. 3** presents calculated densities and viscosities for the injection gas at different pressures at 86°F. The injection-gas density rapidly increases with pressure within the two-phase region, and becomes more than 25 lbm/ft^3 above the bubblepoint of 658 psia. The injection-gas viscosity calculated by use of the Lohrenz-Bray-Clark model (Lohrenz et al. 1964) increases monotonically with pressure.

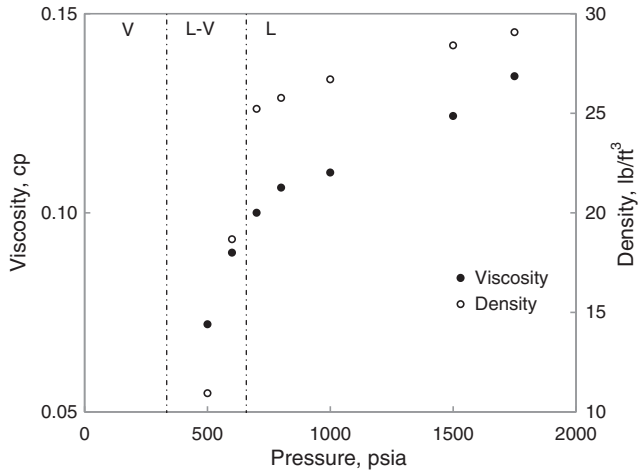

Fig. 3—Viscosities and densities for the injection gas calculated at 86°F. Viscosity calculation is modeled after the Lohrenz-Bray-Clark model (Lohrenz et al. 1964). The injection-gas properties are given in Tables 1 and 2. Two phases are present at pressures between 334 and 658 psia.

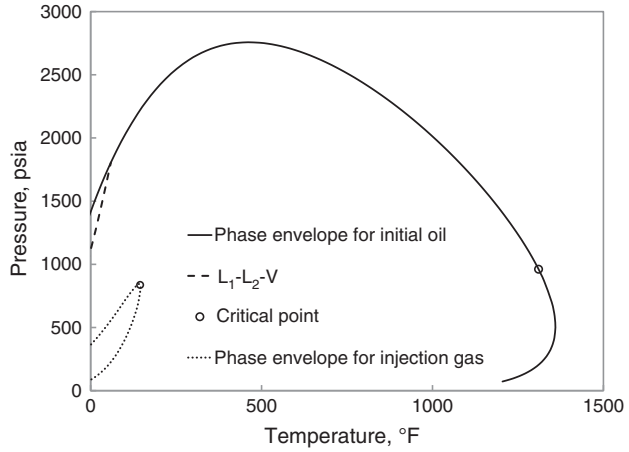

Fig. 2—P/T diagrams of the quaternary oil and injected gas given in Tables 1 and 2. The solid line is the two-phase boundary for the initial oil composition and the dashed line is the three-phase region. The dotted line is the two-phase boundary for the injection gas. The Peng-Robinson EOS is used. The bubblepoint pressure for the oil is 1,953 psia at the reservoir temperature of 86°F. The dewpoint and bubblepoint pressures for the injected gas at 86°F are 334 and 658 psia, respectively.

Fig. 4 gives the pressure/solvent-mole-fraction diagram calculated for mixtures of the oil and the injection gas at 86°F by use of the PVTsim software. Two immiscible liquid phases are present at a wide range of solvent concentrations. Three phases exist between the L_1/L_2 region and the L_1/V region. Mixing of a small amount of the oil with the injection gas causes three-phase behavior at pressures between 211 and 658 psia. Similar phase behavior was presented for Alaskan North Slope heavy oils and solvents in Okuyiga (1992), Godbole et al. (1995), Khataniar et al. (1999),

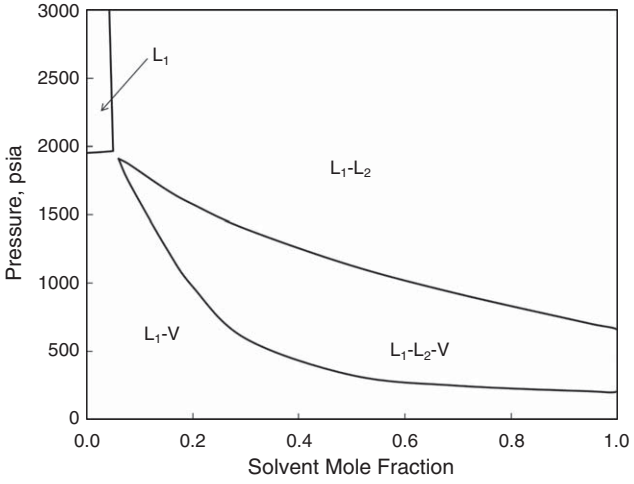

Fig. 4—Pressure/solvent-mole-fraction diagram at 86°F for mixtures of the quaternary oil and the injection gas given in Tables 1 and 2. The oleic, solvent-rich-liquid, and gaseous phases are given as L_1, L_2, and V, respectively.

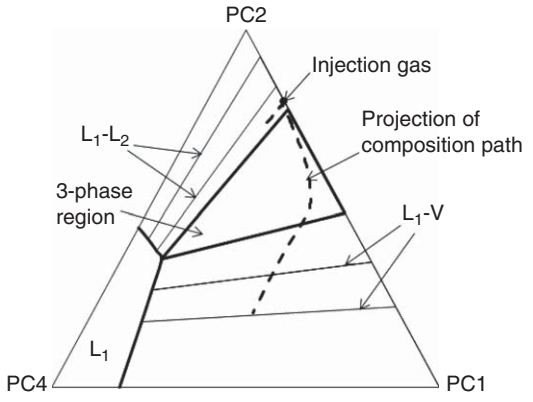

Fig. 5—PC3-free ternary subsystem for the quaternary displacement at 700 psia at 86°F. The bold solid lines are phase boundaries. The solid lines are tie-lines. The dashed line is the projection of the composition at 0.33 HCPVI on this ternary plane. The oil and gas properties are given in Tables 1 and 2.

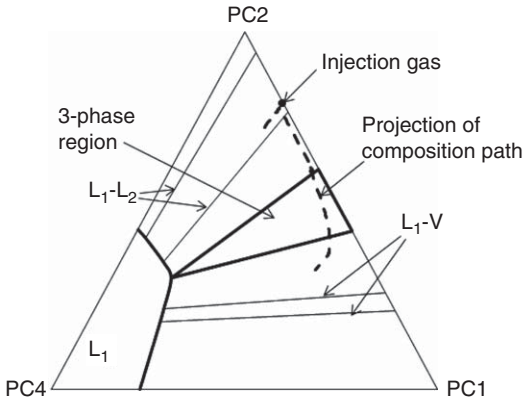

Fig. 6—PC3-free ternary subsystem for the quaternary displacement at 1,000 psia at 86°F. The bold solid lines are phase boundaries. The solid lines are tie-lines. The dashed line is the projection of the composition at 0.33 HCPVI on this ternary plane. The oil and gas properties are given in Tables 1 and 2.

TABLE 3—RESERVOIR PROPERTIES FOR SIMULATIONS OF 1D OIL DISPLACEMENTS

			Corey Model			
Dimensions	$10\times1\times10$ ft^3	Relative Permeability	W	L_1	V	L_2
Number of cells	$1\times1{,}000\times1$	Residual Saturation	0.4	0.2	0.05	0.05
Porosity	0.2	Endpoint Relative Permeability	0.35	0.5	0.65	0.65
Permeability	1,000 md	Exponent	3	3	3	3
		Initial Saturation	0.4	0.6	0	0

McKean et al. (1999), Guler et al. (2001), and Wang et al. (2003). The three-phase behavior in the vicinity of the solvent composition can be seen in ternary subsystems. **Figs. 5 and 6** present phase behavior on the PC3-free ternary subsystems at 700 and 1,000 psia, respectively, at 86°F. The gas composition is near the three-phase region at 700 psia, but not at 1,000 psia.

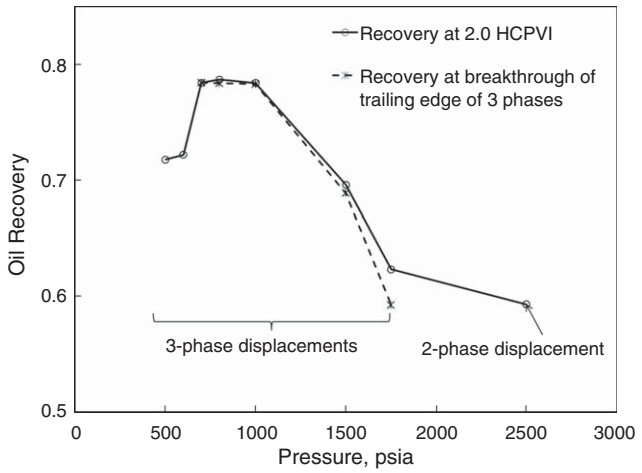

Fig. 7—Oil recovery simulated for the quaternary displacements at different pressures at 86°F. The oil and gas properties are given in Tables 1 and 2. A maximum of 78.69% is observed for recovery at 2.0 HCPVI at 800 psia. At 2.0 HCPVI, the three-phase displacement at 800 psia is 19% more efficient than the two-phase displacement at 2,500 psia. The trailing edge of the three-phase region reaches the outlet at 1.1273 HCPVI at 700 psia, 0.9458 HCPVI at 800 psia, 0.8852 HCPVI at 1,000 psia, 0.7338 HCPVI at 1,500 psia, and 0.6413 HCPVI at 1,750 psia. Oil recovery at breakthrough of the three-phase trailing edge is 78.42% at 700 psia, 78.37% at 800 psia, 78.30% at 1,000 psia, 68.86% at 1,500 psia, and 59.21% at 1,750 psia. Oil displacement by three phases is faster, but less efficient, with increasing pressure.

Table 3 shows the reservoir properties used in simulations in this research. The relative permeability is based on the Corey model. The number of gridblocks is 1,000, with a uniform gridblock size of 1 ft in the displacement direction. The initial water saturation is at the residual saturation of 0.4, and water does not flow in all simulations in this study. Gas injection is continued until the trailing edge of the three-hydrocarbon-phase region reaches the outlet when three phases are present. The quaternary oil displacements are performed at different pressures: 500, 600, 700, 800, 1,000, 1,500, 1,750, and 2,500 psia.

Fig. 7 presents that the displacement efficiencies at 2.0 HCPVI are 71.76, 72.18, 78.42, 78.69, 78.39, 69.59, 62.30, and 59.27% at 500, 600, 700, 800, 1,000, 1,500, 1,750, and 2,500 psia, respectively. A maximum of 78.69% is observed at 800 psia, and the oil recovery at 2.0 HCPVI becomes substantially lower at higher pressures. Three phases are present for the displacements at pressures from 500 to 1,750 psia, but not at 2,500 psia. The 1D oil recovery at 800 psia is 19% more efficient than that at 2,500 psia at 2.0 HCPVI.

Local displacement efficiency at PM conditions depends on the level of miscibility, which affects propagation rates of components. Phase behavior during the displacement is then determined by the resulting compositional variation at the operating pressure and temperature. Fig. 7 also shows oil recovery at breakthrough of the trailing edge of the three-phase region to see the local displacement efficiency by three phases. The trailing edge of the three-phase region reaches the producer at 1.13 HCPVI at 700 psia, 0.95 HCPVI at 800 psia, 0.89 HCPVI at 1,000 psia, 0.73 HCPVI at 1,500 psia, and 0.64 HCPVI at 1,750 psia. Because the trailing edge of the three-phase region is extremely slow at 500 and 600 psia, it is not shown for these pressures. Fig. 7 indicates that the local displacement by three phases becomes less efficient, but propagation of three phases becomes faster with increasing pressure between 700 and 1,750 psia. For example, even though propagation of three phases is faster at 1,750 psia than at 800 psia,

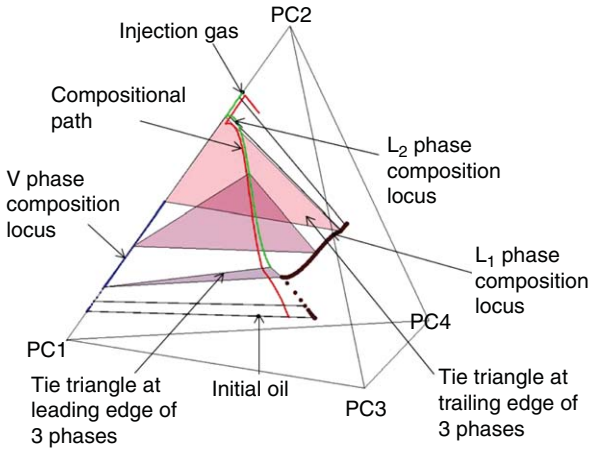

Fig. 8—Phase behavior along the composition path in the quaternary displacement at 700 psia at 86°F. The oil and gas properties are given in Tables 1 and 2. A few tie-lines are shown in the upstream two-phase region and in the downstream two-phase region. A few tie triangles are shown in the three-phase region to show a continuous variation between the leading and trailing edges of the three-phase region.

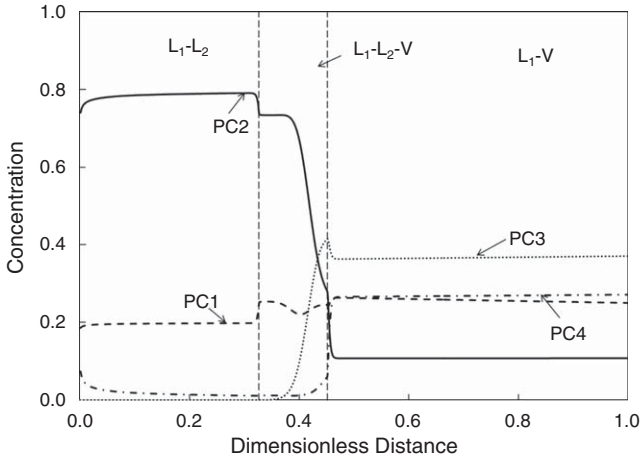

Fig. 9—Simulated component concentrations at 0.33 HCPVI for the quaternary displacement at 700 psia at 86°F. The oil and gas properties are given in Tables 1 and 2.

the local displacement by three phases is less efficient at 1,750 psia than at 800 psia. As a result, the displacement efficiency at a fixed throughput of 2.0 HCPVI is 16% higher at 800 psia than at 1,750 psia, as shown in Fig. 7.

Fig. 8 presents the composition path and phase behavior in the displacement at 700 psia. The phase behavior pattern is observed as follows: V for N_1, L_2 for N_2, and L_2 for N_3. This is also true in the other three-phase displacements presented in later sections. Because the pressure is below the bubblepoint (1,953 psia at 86°F), the initial oil is in the V/L_1 region. The initial high mobility V phase results in formation of an oil bank, as can be seen along the initial oil tie-line [see LaForce and Johns (2010) for detailed explanation of the effect of the initial V-phase saturation on oil recovery]. The tie triangle at the leading edge of the three-phase region is elongated, and the L_1 and L_2 phases are close to each other. The distance between the L_1 and L_2 compositions is 0.0547 at the leading edge. The tie triangle changes its size and shape in the three-phase region, as shown by a few shaded tie triangles in Fig. 8. The tie triangle at the trailing edge of the three-phase region shows that the coexisting phases are highly immiscible with each other. On this tie triangle, the distance is 0.6875 for $\|\underline{x}_{L_1} - \underline{x}_V\|_2$, 0.3956 for $\|\underline{x}_{L_2} - \underline{x}_V\|_2$, and 0.6835 for $\|\underline{x}_{L_1} - \underline{x}_{L_2}\|_2$, where $\underline{x}_j$ is the composition of equilibrium phase j.

The tie-lines in the two-phase regions on the upstream and downstream sides also show their immiscibilities.

Figs. 9 through 12 show the profiles of component concentrations, phase mole fractions, phase saturations, and phase densities, respectively, at 0.33 HCPVI at 700 psia. In Fig. 9, the PC4 concentration is significantly reduced at the three-phase leading edge, and the PC3 concentration becomes essentially zero in the three-phase region. As a result, the tie triangle at the three-phase trailing edge is on the PC3-free ternary subsystem, which is shown in Fig. 5. The amount of the L_1 phase rapidly decreases at the three-phase leading edge in Figs. 10 and 11. The efficient oil displacement is achieved because of the high concentration of the denser injection component PC2 in the three-phase region, as shown in Fig. 9. Fig. 12 shows that the densities of the L_1 and L_2 phases are close to each other at the three-phase leading edge. However, these two phases are still away from each other in composition space with a distance of 0.0547 in Fig. 8.

Fig. 13 shows the profiles of fractional flow at 0.33 HCPVI at 700 psia. The L_2 phase has high fractional-flow values upstream of the three-phase leading edge, indicating that the L_2 phase plays an important role in transport of solvent components during the displacement. **Fig. 14** presents the overall molar flow $\sum_{j=1}^{N_P} \rho_j x_{ij} f_j$ for component i, where ρ_j is the molar density of phase j, x_{ij} is the concentration of component i in phase j, and f_j is the fractional flow of phase j. The overall molar flow of PC2 is higher than that of PC1 upstream of the three-phase leading edge. The fast propagation of

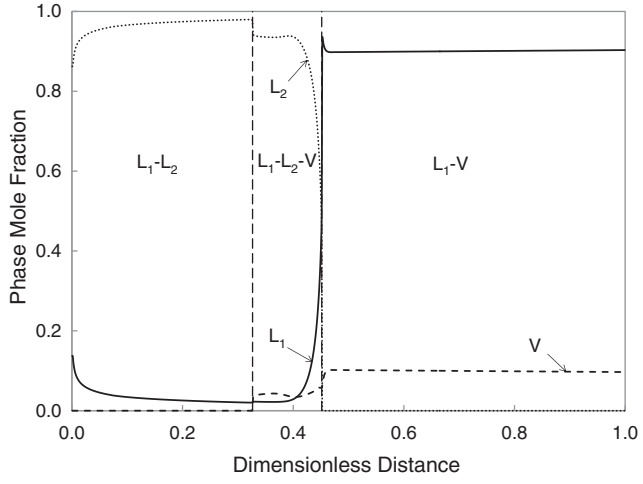

Fig. 10—Simulated phase mole fractions at 0.33 HCPVI for the quaternary displacement at 700 psia at 86°F. The oil and gas properties are given in Tables 1 and 2.

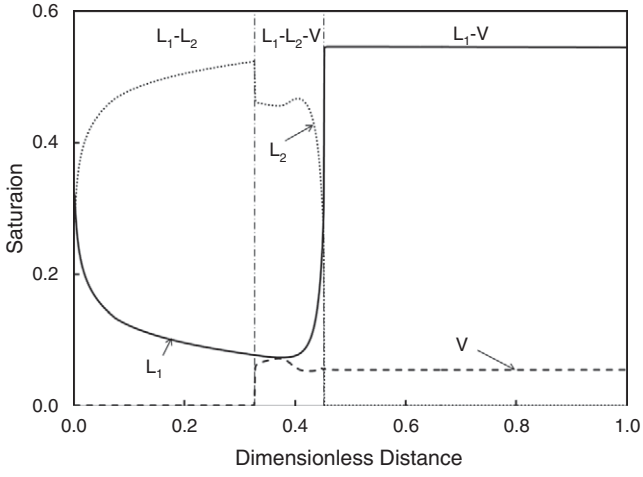

Fig. 11—Simulated phase saturations at 0.33 HCPVI for the quaternary displacement at 700 psia at 86°F. The oil and gas properties are given in Tables 1 and 2.

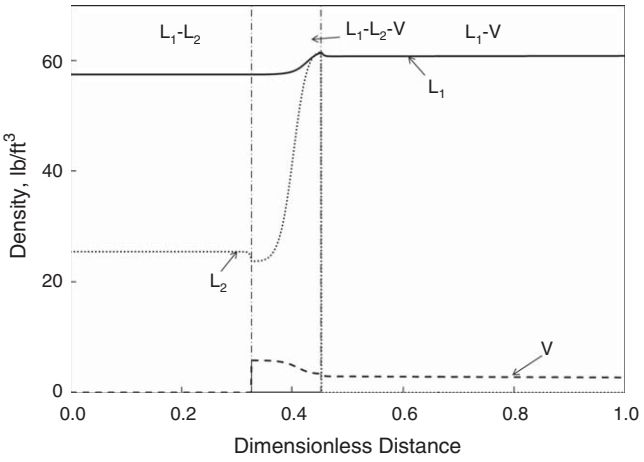

Fig. 12—Simulated phase densities at 0.33 HCPVI for the quaternary displacement at 700 psia at 86°F. The oil and gas properties are given in Tables 1 and 2.

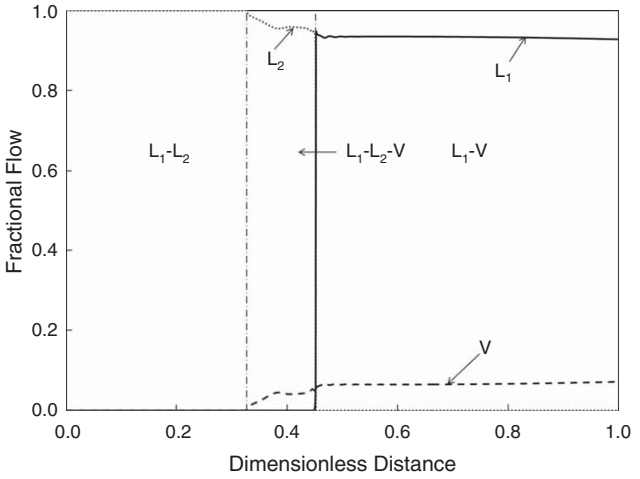

Fig. 13—Simulated phase fractional flow for each phase at 0.33 HCPVI for the quaternary displacement at 700 psia at 86°F. The oil and gas properties are given in Tables 1 and 2.

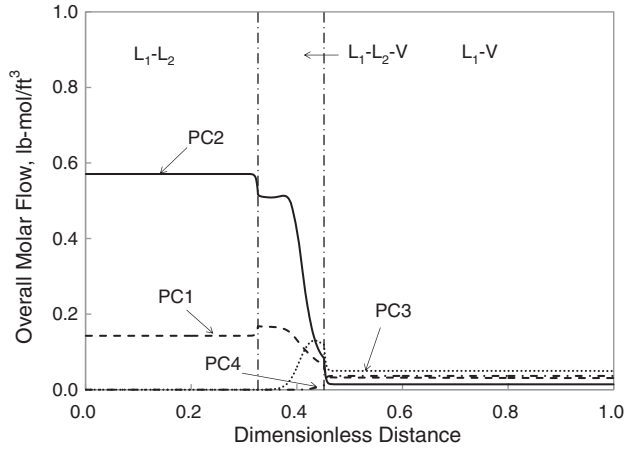

Fig. 14—Simulated overall molar flow for each component at 0.33 HCPVI for the quaternary displacement at 700 psia at 86°F. The oil and gas properties are given in Tables 1 and 2.

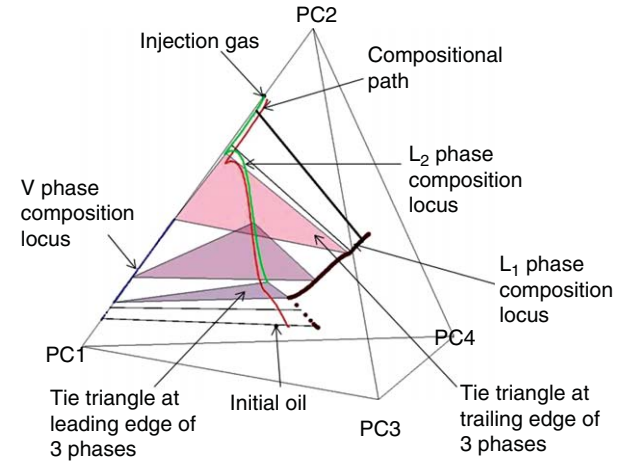

Fig. 15—Phase behavior along the composition path in the quaternary displacement at 1,000 psia at 86°F. The oil and gas properties are given in Tables 1 and 2. A few tie-lines are shown in the upstream two-phase region and in the downstream two-phase region. A few tie triangles are shown in the three-phase region to show a continuous variation between the leading and trailing edges of the three-phase region.

the denser injection component yields efficient oil displacement by rich gas, as presented in Fig. 9.

Fig. 15 gives the composition path in the quaternary diagram at 1,000 psia. **Figs. 16 through 19** show the profiles of component

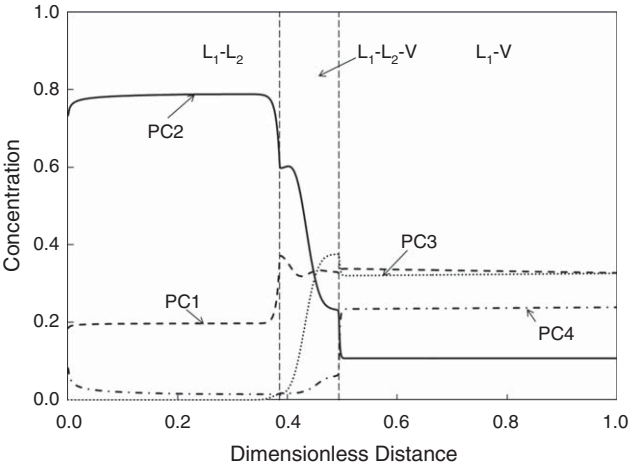

Fig. 16—Simulated component concentrations at 0.33 HCPVI for the quaternary displacement at 1,000 psia at 86°F. The oil and gas properties are given in Tables 1 and 2.

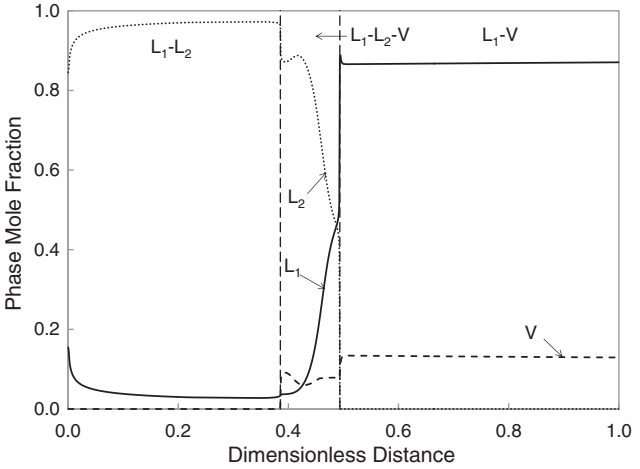

Fig. 17—Simulated phase mole fractions at 0.33 HCPVI for the quaternary displacement at 1,000 psia at 86°F. The oil and gas properties are given in Tables 1 and 2.

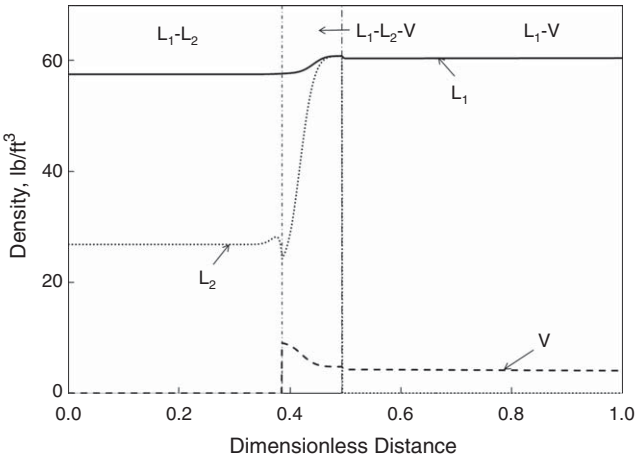

Fig. 18—Simulated phase densities at 0.33 HCPVI for the quaternary displacement at 1,000 psia at 86°F. The oil and gas properties are given in Tables 1 and 2.

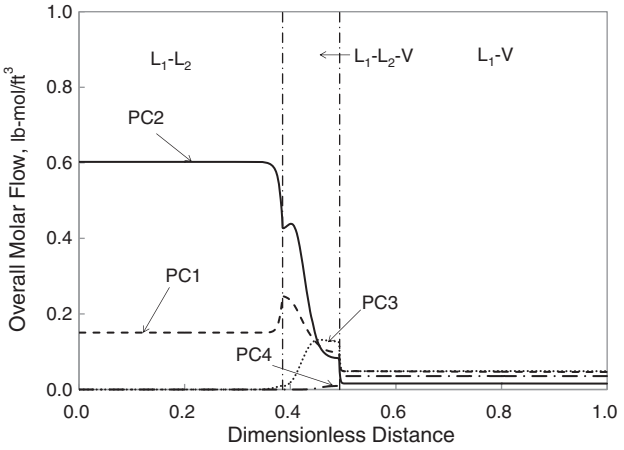

Fig. 19—Simulated overall molar flow for each component at 0.33 HCPVI for the quaternary displacement at 1,000 psia at 86°F. The oil and gas properties are given in Tables 1 and 2.

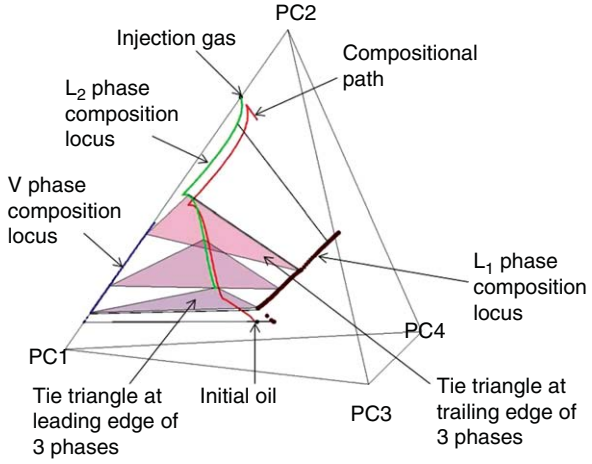

Fig. 20—Phase behavior along the composition path in the quaternary displacement at 1,750 psia at 86°F. The oil and gas properties are given in Tables 1 and 2. A few tie-lines are shown in the upstream two-phase region and in the downstream two-phase region. A few tie triangles are shown in the three-phase region to show a continuous variation between the leading and trailing edges of the three-phase region.

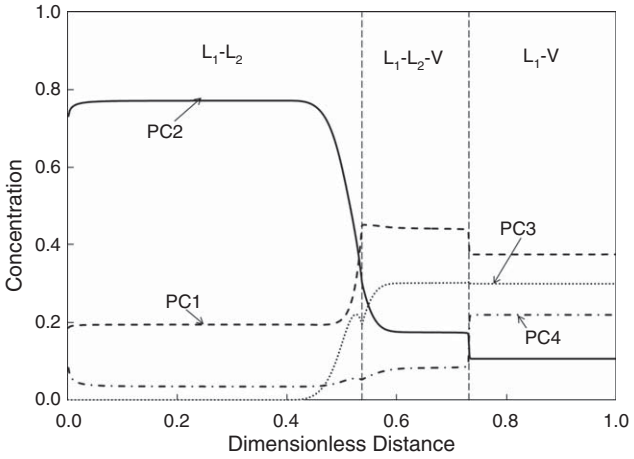

Fig. 21—Simulated component concentrations at 0.33 HCPVI for the quaternary displacement at 1,750 psia at 86°F. The oil and gas properties are given in Tables 1 and 2.

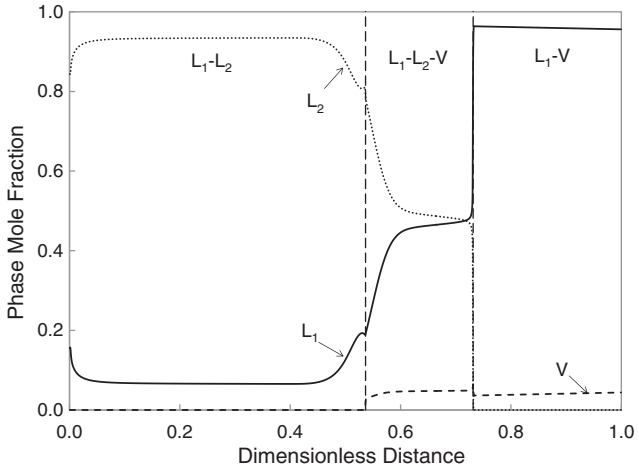

Fig. 22—Simulated phase molar fractions at 0.33 HCPVI for the quaternary displacement at 1,750 psia at 86°F. The oil and gas properties are given in Tables 1 and 2.

concentrations, phase mole fractions, phase densities, and overall molar flows, respectively, at 0.33 HCPVI at 1,000 psia. The same set of figures is given for the displacement at 1,750 psia in **Figs. 20 through 24.** The displacement of PC4 at the three-phase leading edge becomes less efficient with increasing pressure as shown in Figs. 9, 16, and 21. Also, the PC3 concentration upstream of the trailing edge of the three-phase region increases with increasing pressure. Consequently, the tie triangle at the three-phase trailing edge is detached from the PC3-free ternary subsystem in Figs. 15 and 20. Fig. 22 clearly shows the less efficient oil displacement at 1,750 psia compared with Figs. 10 and 17.

The decreasing miscibility level with increasing pressure can be qualitatively seen in density profiles in Figs. 12, 18, and 23. Figs. 20 and 23 indicate that the three-phase equilibria simulated in the displacement at 1,750 psia are not close to CEP tie-lines. The L_2 phase is important in transporting solvent components, as shown in Fig. 13. However, Figs. 14, 19, and 24 show that the overall molar flow of PC2 becomes lower compared with that of PC1 in the three-phase region as pressure increases. The solvent that contacts the L_1 phase at the three-phase leading edge becomes leaner as pressure increases. This solvent propagation behavior with respect to pressure not only reduces the level of miscibility between the L_1 and L_2 phases, but also makes the propagation of the three-phase region faster. Figs. 10 and 22 clearly show the difference in propagation rates of three phases at 700 and 1,750 psia.

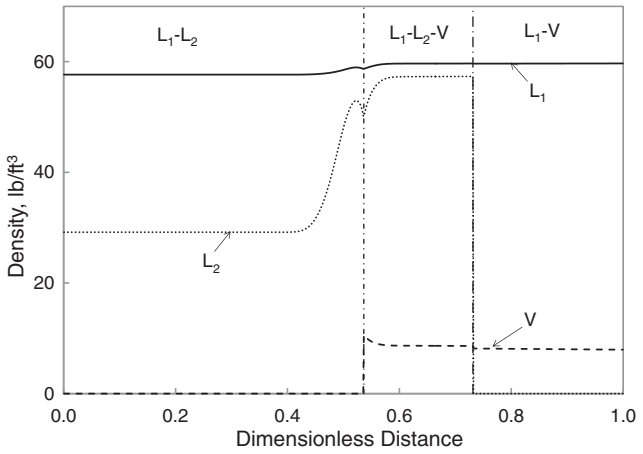

Fig. 23—Simulated phase densities at 0.33 HCPVI for the quaternary displacement at 1,750 psia at 86°F. The oil and gas properties are given in Tables 1 and 2.

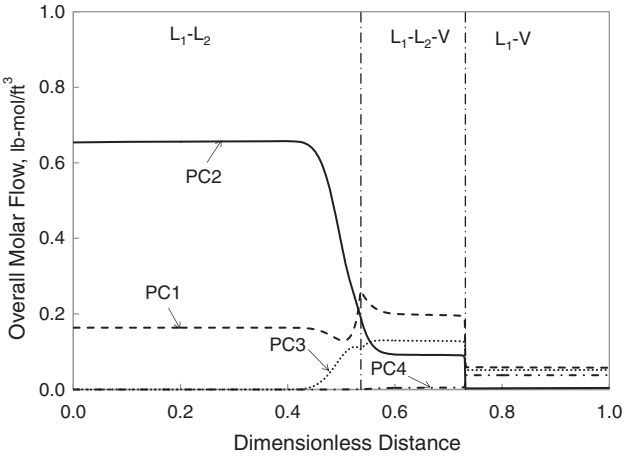

Fig. 24—Simulated overall molar flow for each component at 0.33 HCPVI for the quaternary displacement at 1,750 psia at 86°F. The oil and gas properties are given in Tables 1 and 2.

At 2,500 psia, three phases are not present, and the L_2 phase displaces the oil. This immiscible two-phase flow results in a low displacement efficiency of 59.27% at 2.0 HCPVI. The oil recovery decreases when the three-phase region disappears as pressure increases (Fig. 7).

As mentioned previously, the nonmonotonic trend of oil recovery at a given throughput occurs when the local oil displacement by three hydrocarbon phases becomes less efficient with increasing pressure in the cases considered in this section. The next section, Mass Transfer on Multiphase Transitions, presents simple conditions to quantify the local displacement efficiency by three hydrocarbon phases on the basis of mass conservation for multiphase transitions.

Relative permeability models can significantly affect predictions of solvent-injection processes. Various relative permeability models were tested for simulation of solvent injection for Alaskan heavy oils (Mohanty et al. 1995; Wang and Strycker 2000; Guler et al. 2001; Li et al. 2003; Aghbash and Ahmadi 2012). Guler et al. (2001) showed that the simulation results were sensitive to the relative permeability parameters regardless of which relative permeability model was used. As shown in the figure in Appendix A, the L_2 phase is the intermediate phase that can change the composition between the equilibrium L_1 and V phases. To see the effect of the L_2-phase relative permeability parameters on the quaternary oil recovery, simulations are repeated at 1,000 and 1,750 psia with the injection gas consisting of 20% PC1 and 80% PC2, where the relative permeability parameters for the L_2 phase are set to be the same as those for the L_1 phase (Table 3). **Figs. 25 through 28** show the profiles of component concentrations and phase mole fractions at 0.33 HCPVI at 1,000 and 1,750 psia. The three-phase region propagates slower than the original cases. The effect is more significant at 1,750 psia because the displacement is more immiscible at 1,750 psia than at 1,000 psia. With the modified relative permeability parameters, the oil recovery at 2.0 HCPVI is calculated to be 79.76 and 68.53% at 1,000 and 1750 psia, respectively.

As discussed in the Introduction, gravity segregation and front instability must be taken into account when reservoir-flow patterns of solvent injection are concerned. In Figs. 12, 18, and 23, density differences between the L_1 and L_2 phases are small as also observed by Guler et al. (2001) and Wang et al. (2003). These authors showed that gravity segregation in oil displacement by the L_2 phase in multidimensional simulations was less significant than expected from conventional gas injection. **Fig. 29** compares total relative mobility in the quaternary oil displacements at different pressures at 0.33 HCPVI. As expected, the displacement becomes less unstable as the level of miscibility decreases with increasing pressure. Similar simulation results were presented in Mohanty et al. (1995).

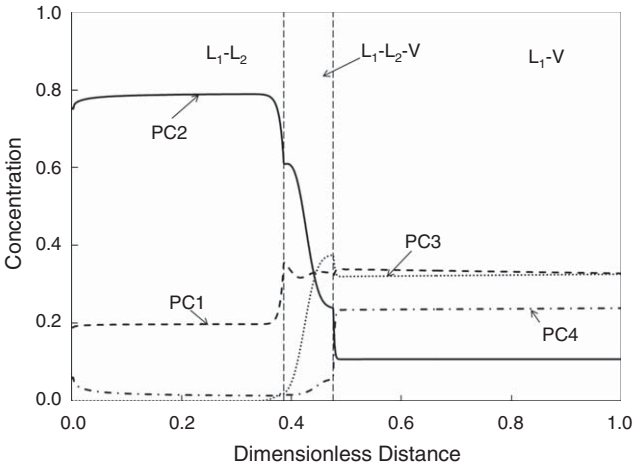

Fig. 25—Simulated component concentrations at 0.33 HCPVI for the quaternary displacement at 1,000 psia at 86°F. The oil and gas properties are given in Tables 1 and 2. The relative permeability parameters for the L_2 phase are set to be the same as those for the L_1 phase.

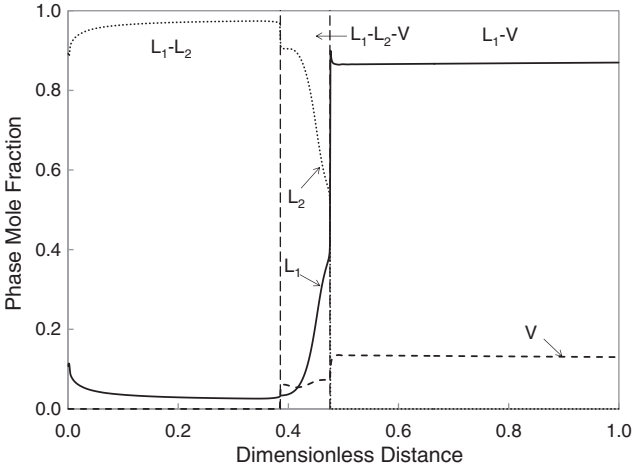

Fig. 26—Simulated phase mole fractions at 0.33 HCPVI for the quaternary displacement at 1,000 psia at 86°F. The oil and gas properties are given in Tables 1 and 2. The relative permeability parameters for the L_2 phase are set to be the same as those for the L_1 phase.

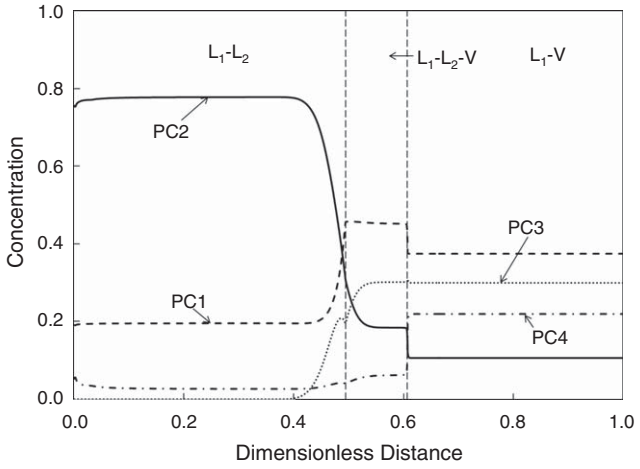

Fig. 27—Simulated component concentrations at 0.33 HCPVI for the quaternary displacement at 1,750 psia at 86°F. The oil and gas properties are given in Tables 1 and 2. The relative permeability parameters for the L_2 phase are set to be the same as those for the L_1 phase.

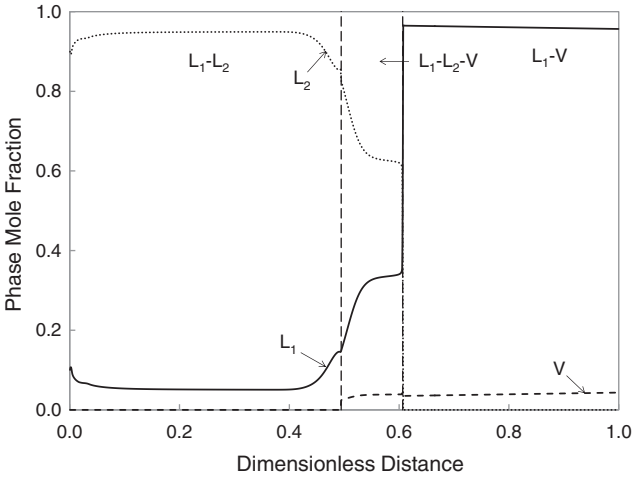

Fig. 28—Simulated phase mole fractions at 0.33 HCPVI for the quaternary displacement at 1,750 psia at 86°F. The oil and gas properties are given in Tables 1 and 2. The relative permeability parameters for the L_2 phase are set to be the same as those for the L_1 phase.

An approximate Péclet number is 2,000 for the 1D quaternary displacements described previously, where the IMPEC simulator was used with 1,000 equally spaced gridblocks and small timestep sizes [see Johns et al. (2000) for an explanation of the approximation]. As explained in Jessen et al. (2004), numerical dispersion can significantly affect simulation results for oil displacement by gas. The quaternary displacements at 1,000 and 1,750 psia were repeated with two different numerical-dispersion levels, one with 250 gridblocks and the other with 50 gridblocks. They correspond to approximate Péclet numbers of 500 and 100, respectively. In the displacements at 1,000 psia, oil recoveries simulated at 2.0 HCPVI are 78.39% with 1,000 gridblocks, 72.24% with 250 gridblocks, and 59.24% with 50 gridblocks. In the displacements at 1,750 psia, they are 62.30% with 1,000 gridblocks, 60.65% with 250 gridblocks, and 55.03% with 50 gridblocks. The effect of numerical dispersion is more significant at 1,000 psia than at 1,750 psia because the level of miscibility is higher at 1,000 psia, as described previously in this section. A sensitivity study of simulation results to numerical dispersion can be also found in Okuno (2009) for low-temperature CO_2 floods involving three-hydrocarbon-phase behavior.

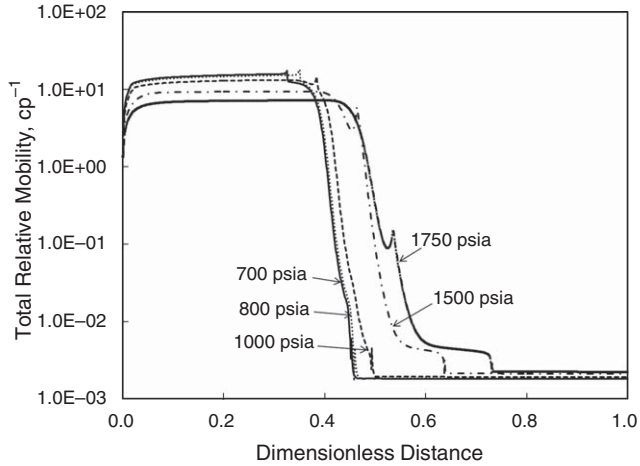

Fig. 29—Simulated total relative mobility at 0.33 HCPVI for the quaternary displacements at 700, 800, 1,000, 1,500, and 1,750 psia at 86°F. The oil and gas properties are given in Tables 1 and 2.

Mass Transfer on Multiphase Transitions

Our investigation in this section is focused on phase transitions between two and three phases in three-hydrocarbon-phase displacement. An analysis of mass conservation is presented for multiphase transitions in three-hydrocarbon-phase displacements. Material-balance equations for 1D dispersion-free compositional flow are discretized in Appendix B for a multiphase transition between N_P^U and N_P^D phases, where N_P^U and N_P^D are the numbers of phases on the upstream and downstream sides, respectively. The resulting equation (Eq. B-5) is of the identical form with the generalized jump conditions (Eq. B-7), which can be used in the MOC solution of multiphase flow. Eq. B-5 is more general than Eq. B-7, and can be used to analyze interphase mass transfer on multiphase transitions in the presence of numerical dispersion.

Eqs. B-5 and B-7 state that a multiphase transition between N_P^U and N_P^D phases occurs through an intersection between the extensions of the two tie simplexes defined by $\underline{x}_j^U$ ($j=1, 2, \ldots, N_P^U$) and $\underline{x}_k^D$ ($k=1, 2, \ldots, N_P^D$), where $\underline{x}_j$ is the composition of equilibrium phase j. For a phase transition between one and two phases with a shock, this statement reduces to the well-known result of Helfferich (1981)—that a shock between one and two phases must occur on the tie-line extension. A phase transition between two and three phases occurs through an intersection between the tie-line extension and the tie-triangle-extension plane. Redistribution of components on the phase transition then satisfies the material balance for the two and three phases.

The phase labeling given in Fig. 1 is used to discuss an efficient redistribution of components on multiphase transition. The two nonoleic phases are partially miscible with the L_1 phase in the three-phase displacements studied in this research. However, the two nonoleic phases can collectively achieve high displacement efficiency if two conditions are satisfied on the phase transitions between two and three phases. The first condition is that the appearance of the N_2 phase should occur by splitting the L_1 phase in the downstream two-phase region into the L_1 and N_2 phases in the three-phase region. The second condition is that the N_1 and N_2 phases in the three-phase region should merge into the N_3 phase in the upstream two-phase region.

It is easy to derive mathematical expressions for these conditions. For instance, derivation for the first condition starts with Eq. B-5 for the leading edge of the three-phase region [i.e., $\sum_j \gamma_j^U \underline{c}_j^U = \sum_k \gamma_k^D \underline{c}_k^D$, where $j=(L_1, N_1, N_2)$ and $k=(L_1, N_1)$]. The first condition is

$$\left\| \gamma_{N_1}^U \underline{c}_{N_1}^U - \gamma_{N_1}^D \underline{c}_{N_1}^D \right\|_2 < \varepsilon, \quad \ldots\ldots\ldots\ldots\ldots\ldots\ldots\ldots (1)$$

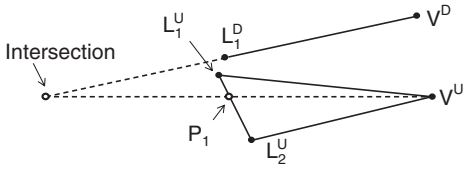

Fig. 30—Schematic of phase transition in composition space at the leading edge of the three-phase region. It is assumed that there are L_1 and V downstream, and L_1, L_2, and V upstream of the phase transition. Black dots indicate equilibrium phase compositions. The superscripts D and U stand for downstream and upstream, respectively. Redistribution of components between two and three phases occurs through the intersection. The composition of the P_1 pseudophase is defined where the line connecting the intersection and the V^U phase composition intersects (the extension of) the L_1/L_2 edge of the tie triangle.

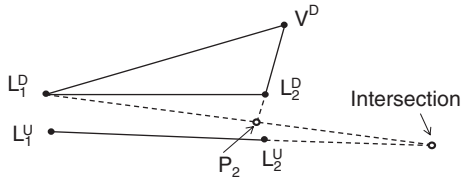

Fig. 31—Schematic of phase transition in composition space at the trailing edge of the three-phase region. It is assumed that there are L_1 and L_2 upstream, and L_1, L_2, and V downstream of the phase transition. Black dots indicate equilibrium phase compositions. The superscripts D and U stand for downstream and upstream, respectively. Redistribution of components between two and three phases occurs through the intersection. The composition of the P_2 pseudophase is defined where the line connecting the intersection and the L_1^D phase composition intersects (the extension of) the V/L_2 edge of the tie triangle.

such that

$$\gamma^U_{N_2}\underline{c}^U_{N_2} + \gamma^U_{L_1}\underline{c}^U_{L_1} \approx \gamma^D_{L_1}\underline{c}^D_{L_1}. \quad \ldots\ldots\ldots\ldots\ldots\ldots (2)$$

Substitution of Eq. 1 into Eq. B-5 yields Eq. 2. Eq. 2 states that redistribution of components must occur between the L_1 and N_2 phases. Similarly, the second condition is

$$\left\|\gamma^D_{L_1}\underline{c}^D_{L_1} - \gamma^U_{L_1}\underline{c}^U_{L_1}\right\|_2 < \varepsilon, \quad \ldots\ldots\ldots\ldots\ldots\ldots (3)$$

such that

$$\gamma^D_{N_1}\underline{c}^D_{N_1} + \gamma^D_{N_2}\underline{c}^D_{N_2} \approx \gamma^U_{N_3}\underline{c}^U_{N_3}. \quad \ldots\ldots\ldots\ldots\ldots\ldots (4)$$

Summation of Eqs. 3 and 4 yields Eq. B-5 for the trailing edge of the three-phase region. Eq. 4 states that the two nonoleic phases in the three-phase region should merge into a nonoleic phase in the upstream two-phase region.

Eqs. 1 and 3 can be rewritten by use of phase compositions as follows:

$$\delta^L = \left\|\Gamma^U_{N_1}\underline{x}^U_{N_1} - \Gamma^D_{N_1}\underline{x}^D_{N_1}\right\|_2 < \varepsilon, \quad \ldots\ldots\ldots\ldots\ldots\ldots (5)$$

$$\delta^T = \left\|\Gamma^U_{L_1}\underline{x}^U_{L_1} - \Gamma^D_{L_1}\underline{x}^D_{L_1}\right\|_2 < \varepsilon. \quad \ldots\ldots\ldots\ldots\ldots\ldots (6)$$

The Γ_j ($j=1, 2,\ldots, N_P$) parameters determine the relative location of the N_P-phase tie simplex and an intersection involved in the phase transition. The conditions specific to the quaternary displacements in the previous section are as follows: $\delta^L = \left\|\Gamma^U_V\underline{x}^U_V - \Gamma^D_V\underline{x}^D_V\right\|_2 < \varepsilon$ and $\delta^T = \left\|\Gamma^U_{L_1}\underline{x}^U_{L_1} - \Gamma^D_{L_1}\underline{x}^D_{L_1}\right\|_2 < \varepsilon$. **Figs. 30 and 31** give schematics for the phase transitions at the leading and trailing edges of the three-phase region, respectively. These schematics indicate that a phase transition between two and three phases involves an intersection of the tie-line extension and the tie-triangle extension as described in Appendix B.

Once the tie-line and tie triangle involved in a phase transition (e.g., the tie-line downstream and the tie triangle upstream in Fig. 30) are given, we can calculate an intersection of them. The location of the intersection relative to the tie-line then gives the Γ_j ($j=V$ and L_1) parameters on the tie-line extension. Thus, $\underline{z}^{\text{int}} = \Gamma^D_V\underline{x}^D_V + \Gamma^D_{L_1}\underline{x}^D_{L_1}$, where $\Gamma^D_V + \Gamma^D_{L_1} = 1.0$ and $\underline{z}^{\text{int}}$ is the intersection composition. Similarly, the location of the same intersection relative to the tie triangle gives the Γ_j ($j=V$, L_1, and L_2) parameters on the tie-triangle extension. Thus, $\underline{z}^{\text{int}} = \Gamma^U_V\underline{x}^U_V + \Gamma^U_{L_1}\underline{x}^U_{L_1} + \Gamma^U_{L_2}\underline{x}^U_{L_2}$, where $\Gamma^U_V + \Gamma^U_{L_1} + \Gamma^U_{L_2} = 1.0$. Calculation of δ^L and δ^T will be conducted by use of this procedure for the quaternary displacements later in this section, and for the West Sak oil displacements in the subsequent section.

Fig. 30 shows a pseudophase P_1, where the line connecting the intersection and the V^U phase composition intersects (the extension of) the L_1/L_2 edge of the tie triangle. We can consider that redistribution of components from two to three phases occurs in three steps: the L_1 and V phases on the downstream tie-line form the intersection composition; the intersection composition forms two phases, the P_1 and V phases, on the upstream tie triangle; and the P_1 phase splits into the L_1 and L_2 phases on the tie triangle. Fig. 31 shows a pseudophase P_2, where the line connecting the intersection and the L_1 phase composition intersects the extension of the L_2/V edge of the tie triangle. Redistribution of components from three to two phases occurs in the following three steps: the L_2 and V phases form the P_2 phase on the tie-triangle extension downstream; the P_2 and L_1 phases form the intersection composition; and the intersection composition forms the L_1 and V phases on the tie-line upstream. Fig. 31 shows a more general case, where the pseudophase is outside the tie triangle.

Eqs. 2 and 4 become exact when the pseudotie-line on the tie triangle and the tie-line coincide. In Fig. 30, for example, the L_1^U and L_2^U phases on the tie triangle merge into the L_1^D phase on the tie-line without affecting the other coexisting V phase when the P_1/V^U pseudotie-line and the L_1^D/V^D tie-line coincide. This can occur for phase transitions on a CEP tie-line and on an edge of a tie triangle. LaForce and Orr (2009) presented the latter type of phase transitions in analytical solutions for oil displacements, which cross the boundary between two and three phases without a shock.

The efficient mass transfer on multiphase transitions near the UCEP and LCEP tie-lies was described for low-temperature CO_2 floods in Okuno et al. (2011). This can be interpreted by use of the limiting case mentioned previously. As the LCEP is approached in Fig. 30, the L_1 and L_2 phases on the upstream tie triangle become closer to each other. The P_1/V pseudotie-line then becomes closer to the L_1/V tie-line downstream. Similarly, the P_2/L_1 pseudotie-line becomes closer to the upstream L_1/L_2 tie line when the composition path goes near the UCEP tie-line. Eqs. 5 and 6 are naturally satisfied with small ε values for such low-temperature CO_2 floods. However, this does not occur for the efficient displacements by use of the quaternary system in the previous section. For example, Fig. 15 shows tie triangles along the composition path that are not close to CEP tie-lines.

We calculate the distances given in Eqs. 5 and 6 (i.e., $\delta^L = \|\Gamma^U_{N_1}\underline{x}^U_{N_1} - \Gamma^D_{N_1}\underline{x}^D_{N_1}\|_2$ and $\delta^T = \|\Gamma^U_{L_1}\underline{x}^U_{L_1} - \Gamma^D_{L_1}\underline{x}^D_{L_1}\|_2$) for the quaternary displacements at 700, 800, 1,000, 1,500, and 1,750 psia. **Fig. 32** shows that δ^L and δ^T decrease as pressure decreases for these displacements; that is, mass transfer on multiphase transitions occurs most efficiently at 700 psia. The L_1 phase in the leading two-phase region splits into the L_1 and L_2 phases in the three-phase region, and the L_2 and V phases in the three-phase region merge efficiently into the L_2 phase in the trailing two-phase region. Consequently, the oil recovery at the breakthrough of the three-phase trailing edge exhibits the highest efficiency at 700 psia in Fig. 7.

The distances, δ^L and δ^T, are also calculated for quaternary displacements with different gas-enrichment levels. Injection gas consists of PC1 and PC2, but different levels of gas enrichment use different mixing ratios. Reservoir properties are given in Table 3. The displacement pressure is 1,500 psia, and the reservoir

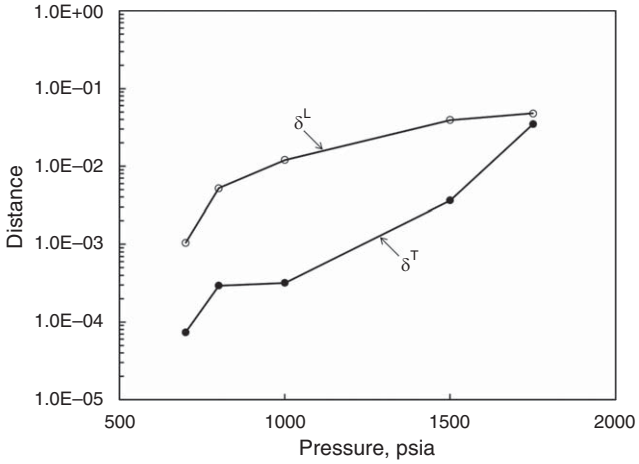

Fig. 32—The distance parameters δ^L and δ^T (Eqs. 5 and 6) calculated for the quaternary displacements at 700, 800, 1,000, 1,500, and 1,750 psia. For these displacements, local displacement by three phases becomes more efficient for lower pressure. Oil recovery at breakthrough of the three-phase trailing edge is 78.42% at 700 psia, 78.37% at 800 psia, 78.30% at 1,000 psia, 68.86% at 1,500 psia, and 59.21% at 1,750 psia, as shown in Fig. 7.

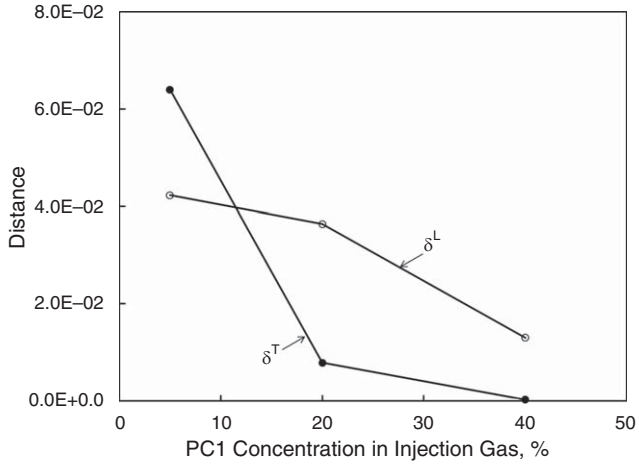

Fig. 33—The distance parameters δ^L and δ^T (Eqs. 5 and 6) calculated for the quaternary displacements at different enrichment levels at 1,500 psia and 86°F. For these displacements, local displacement by three phases becomes more efficient for higher PC1 dilution. Oil recovery at breakthrough of the three-phase trailing edge is 65.2% at 5% PC1, 66.8% at 20% PC1, and 66.9% at 40% PC1, as shown in Fig. 34.

temperature is 86°F. Three phases are present for displacements with high enrichment levels. **Fig. 33** presents that local displacement by three phases becomes more efficient with decreasing enrichment. At 40% PC1, δ^L is 1.3×10^{-2} and δ^T is 2.5×10^{-4}. **Fig. 34** shows that displacement efficiency at 2.0 HCPVI exhibits a maximum of 68.39% for the PC1 concentration of 20% in the injection gas. Three-phase displacement with less enrichment achieves higher local displacement efficiency, but it becomes slower. The trailing edge of three phases reaches the outlet at 0.709 HCPVI at 5% PC1, 0.724 HCPVI at 20% PC1, and 0.768 HCPVI at 40% PC1. The three-phase region is also present at 60% PC1, but its propagation is extremely slow. Oil recovery at a given throughput depends not only on local displacement efficiency by three phases, but also on the propagation rate of three phases. A maximum oil recovery at 2.0 HCPVI in Fig. 34 is a result of the balance between the local displacement efficiency and the propagation rate of three hydrocarbon phases.

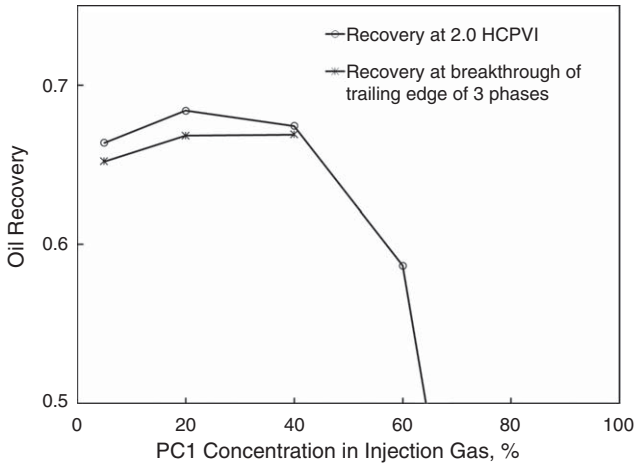

Fig. 34—Oil recovery simulated for the quaternary displacements at different gas-enrichment levels at 1,500 psia and 86°F. The fluid properties are given in Tables 1 and 2. A maximum of 68.39% is observed for recovery at 2.0 HCPVI at a PC1 concentration of 20%. The trailing edge of the three-phase region reaches the outlet at 0.709 HCPVI at 5% PC1, 0.724 HCPVI at 20% PC1, and 0.768 HCPVI at 40% PC1. Oil recovery at breakthrough of the three-phase trailing edge is 65.2% at 5% PC1, 66.8% at 20% PC1, and 66.9% at 40% PC1. Oil displacement by three phases is more efficient, but slower, with increasing PC1 dilution. The three-phase region is also present at 60% PC1, but its propagation is extremely slow.

Case Study for West Sak Oil Displacement With Enriched Gas

Nonmonotonic oil recovery at a given throughput with respect to gas enrichment has been reported for the West Sak oil displacement (DeRuiter et al. 1994; Mohanty et al. 1995). However, its detailed mechanism is uncertain in the literature, as mentioned in the Introduction. In this section, the distance conditions derived in the preceding section are applied to the West Sak oil displacement with enriched gas.

The West Sak oil is characterized by use of the Peng-Robinson EOS on the basis of data available in Okuyiga (1992) (Xu 2012). The 15-component model given in **Table 4** includes eight pseudocomponents for the C_{7+} fraction. The Lohrenz-Bray-Clark model (Lohrenz et al. 1964) is used for viscosity calculations. The oil gravity is calculated to be approximately 21°API. **Fig. 35** presents the P/T diagram for the oil. The saturation pressure is 1,197 psia at the reservoir temperature of 65°F.

The injection gas consists of two gaseous mixtures: the rich-gas mixture of 35 mol% ethane, 34 mol% propane, and 31 mol% *n*-butane, and the lean-gas mixture of 84 mol% C_1, 9 mol% ethane, 6 mol% propane, and 1 mol% *n*-butane. Oil displacements are simulated for eight different enrichment levels. The resulting enriched gases are referred to by use of their C_1 concentrations. **Fig. 36** shows the pressure/solvent-mole-fraction diagram for the reservoir oil and the injection gas with 60% C_1 concentration at 65°F. Three phases are present at high solvent concentrations at the operating pressure range. The L_1/L_2 immiscibility persists to high pressure. The reservoir properties used are given in Table 3. The displacement pressure is 1,500 psia.

As mentioned in the Introduction, three-phase behavior bounded by CEPs has been observed for *n*-alkane binaries; C_1/nC_6, C_1/nC_7, C_2/*n*-alkanes from nC_{18} to nC_{25}; and C_3/*n*-alkanes heavier than nC_{30}. Mixtures of the rich-gas components—C_2, C_3, and C_4—likely tend to cause three-phase behavior with the C_{7+} fraction of the oil at reservoir temperatures.

Fig. 37 presents oil recovery at different gas enrichments at 1.0, 1.5, and 2.0 HCPVI. Three hydrocarbon phases are present in the displacements at C_1 concentrations in the injection gas between 50 and 70%. At a C_1 concentration of 53%, oil recovery is 84.29% at 1.0 HCPVI, 90.18% at 1.5 HCPVI, and 91.53% at 2.0 HCPVI. The injection gas with this C_1 concentration yields an optimum displacement for a fixed throughput in Fig. 37. Mohanty

TABLE 4—PROPERTIES OF THE WEST SAK OIL (Xu 2012)

Components	Oil (mol%)	Rich Gas (mol%)	Lean Gas (mol%)	Molecular Weight	T_c (°R)	P_c (psia)	V_c (ft^3/lbm-mol)	Acentric Factor	Binary Interaction CO_2	Binary Interaction C_1
CO_2	0.22	0.0	0.0	44.01	547.56	1069.87	1.51	0.2250	0.00	0.180
C_1	27.47	0.0	84.0	16.04	343.08	667.20	1.59	0.0080	0.18	0.000
C_2	0.66	35.0	9.0	30.07	549.72	708.35	2.37	0.0980	0.18	0.010
C_3	0.15	34.0	6.0	44.10	665.64	615.76	3.25	0.1520	0.18	0.010
C_4	0.27	31.0	1.0	58.12	765.36	551.10	4.08	0.1930	0.18	0.010
C_5	0.19	0.0	0.0	72.15	845.28	489.38	4.87	0.2510	0.18	0.010
C_6	0.29	0.0	0.0	86.18	913.32	430.59	5.93	0.2960	0.18	0.010
$C_{7–9}$	3.22	0.0	0.0	105.65	1060.48	418.62	8.29	0.3697	0.05	0.007
$C_{10–14}$	17.95	0.0	0.0	157.72	1220.50	323.21	8.41	0.5389	0.05	0.007
$C_{15–18}$	13.21	0.0	0.0	210.19	1349.89	274.12	14.54	0.6992	0.05	0.007
$C_{19–23}$	10.91	0.0	0.0	259.06	1424.95	251.96	19.02	0.8373	0.05	0.007
$C_{24–27}$	5.84	0.0	0.0	302.85	1493.37	242.09	22.88	0.9500	0.05	0.007
$C_{28–33}$	6.60	0.0	0.0	344.37	1550.96	230.14	22.74	1.0453	0.05	0.007
$C_{34–40}$	4.42	0.0	0.0	389.77	1629.48	223.31	44.05	1.1345	0.05	0.007
C_{41+}	8.60	0.0	0.0	600.00	1914.78	182.82	53.57	1.2120	0.05	0.007

et al. (1995) showed nonmonotonic recovery trends that are more obvious in their slimtube experiments and numerical simulations.

Fig. 38 shows the distances given in Eqs. 5 and 6 for the displacements at 50, 53, 55, and 60% C_1 concentrations. The distances decrease for leaner injection gas. At the C_1 concentration of 60%, δ^L is 9.0×10^{-3} and δ^T is 3.9×10^{-4}. These results indicate that the local displacement by three hydrocarbon phases becomes more efficient with decreasing gas enrichment. The injection gas with the C_1 concentration of 60% gives the maximum efficiency of three-phase local displacement (Fig. 37). Oil recovery at breakthrough of the three-phase trailing edge is 90.4% at 50% C_1, 92.0% at 53% C_1, and 97.4% at 60% C_1.

However, propagation of three phases is slower at higher C_1 concentrations. The trailing edge of three phases reaches the outlet at 2.15, 2.34, 2.73, and 14.94 HCPVI at the C_1 concentrations of 50, 53, 55, and 60%, respectively. We could not observe the three-phase trailing edge at the outlet for the C_1 concentration of 70%. Because of the slow propagation of three phases, oil recovery is 69.01% at 1.0 HCPVI, 85.71% at 1.5 HCPVI, and 87.75% at 2.0 HCPVI at the C_1 concentration of 60%.

Local displacement by three phases is more efficient, but propagation of three phases is slower, for leaner injection gas for these three-phase displacements. These two factors determine a maximum in oil recovery at a given throughput in Fig. 37. A maximum recovery at a given throughput will occur at a different dilution level when different reservoir and/or fluid properties are used.

Conclusions

We investigated local efficiency of three-hydrocarbon-phase displacement of oil. Mathematical conditions were derived for efficient redistribution of components on multiphase transitions between two and three phases. These conditions were used to explain nonmonotonic oil recovery at a given throughput with respect to gas enrichment, which has been reported for the West Sak oil in the literature. Conclusions are as follows:

- Oil recovery in a PM displacement depends on two factors: local displacement efficiency and component propagation rates. Nonmonotonic oil recovery at a given throughput can occur when local displacement by three hydrocarbon phases becomes more efficient, but slower, with decreasing pressure or decreasing gas enrichment. This was confirmed by use of fine-scale simulations of quaternary displacements and the West Sak oil displacements. A maximum in oil recovery at a given throughput occurs as a consequence of the balance between the local displacement efficiency and the propagation rate of three hydrocarbon phases.
- Local displacement efficiency by three hydrocarbon phases depends significantly on how components are redistributed on

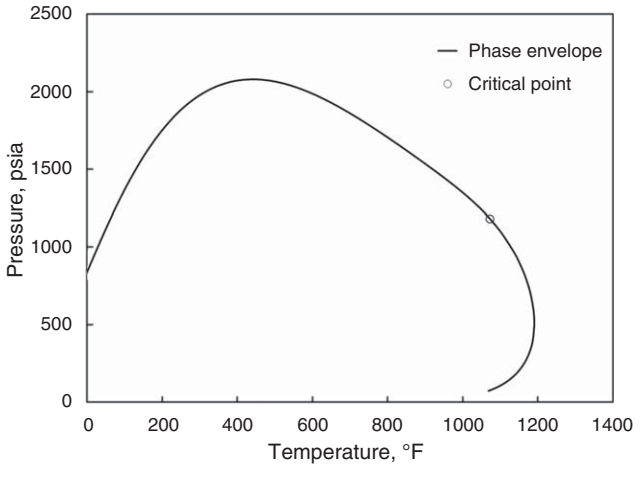

Fig. 35—P/T diagram of the West Sak oil given in Table 4. The Peng-Robinson EOS is used. The saturation pressure is 1,197 psia at the reservoir temperature of 65°F.

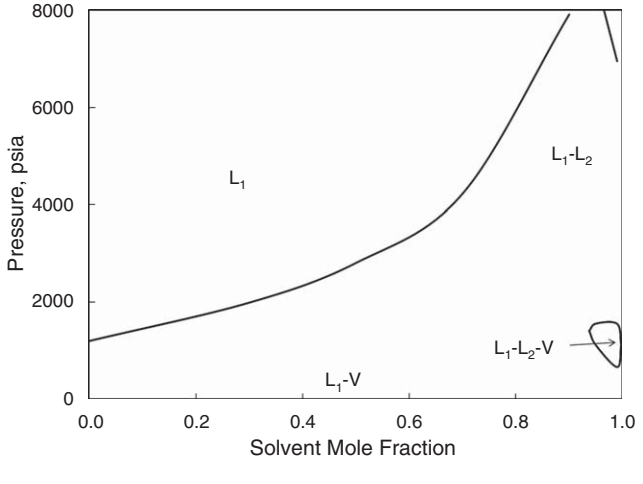

Fig. 36—Pressure/solvent-mole-fraction diagram at 65°F for mixtures of the West Sak oil and the injection gas with 60% C_1. Fluid properties used are given in Table 4. The oleic, solvent-rich-liquid, and gaseous phases are given as L_1, L_2, and V, respectively.

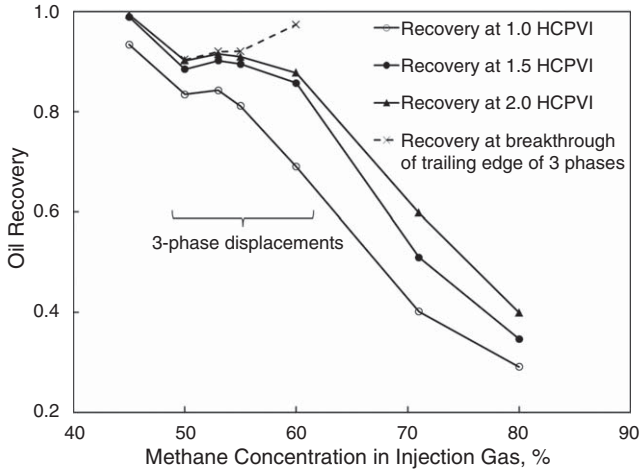

Fig. 37—Oil recovery simulated for the West Sak displacements at different gas-enrichment levels at 1,500 psia and 65°F. The fluid properties are given in Table 4. A maximum of 91.53% is observed for recovery at 2.0 HCPVI at a C_1 concentration of 53%. The trailing edge of the three-phase region reaches the outlet at 2.15 HCPVI at 50% C_1, 2.34 HCPVI at 53% C_1, 2.73 HCPVI at 55% C_1, and 14.94 HCPVI at 60% C_1. Oil recovery at breakthrough of the three-phase trailing edge reaches 97.4% at 60% C_1. Oil displacement by three phases is more efficient, but slower, with decreasing gas enrichment.

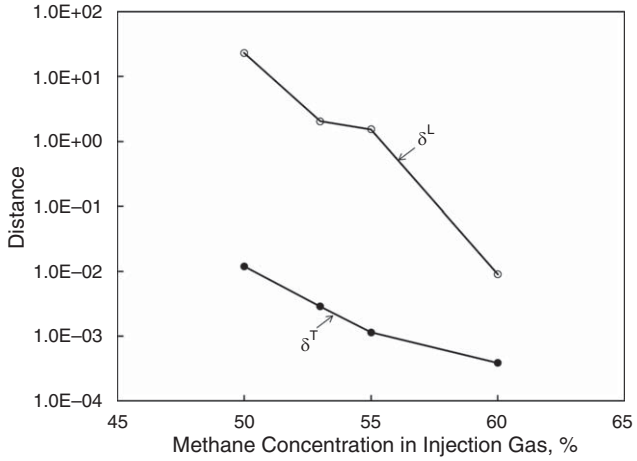

Fig. 38—The distance parameters δ^L and δ^T (Eqs. 5 and 6) calculated for the West Sak displacements at different enrichment levels at 1,500 psia and 65°F. For these displacements, local displacement by three phases becomes more efficient for less gas enrichment. Oil recovery at breakthrough of the three-phase trailing edge is 90.4% at 50% C_1, 92.0% at 53% C_1, and 97.4% at 60% C_1, as shown in Fig. 37.

multiphase transitions between two and three phases. At the leading edge of the three-phase region, the second nonoleic phase should appear from the oleic phase of the downstream two-phase region. At the trailing edge of the three-phase region, two nonoleic phases of the three-phase region should merge into the nonoleic phase of the upstream two-phase region.

- The distances defined in Eqs. 5 and 6 for efficient multiphase transitions can correctly identify the local displacement efficiency by three hydrocarbon phases. The distances were successfully used to explain the quaternary displacements and the West Sak oil displacements that exhibit nonmonotonic oil recovery. The distance conditions can also explain the efficient displacement through near-CEP behaviors presented in prior research on low-temperature CO_2 floods.
- Partially miscible displacement of oil by two nonoleic phases can be collectively efficient, even if they are individually immiscible with oil. The West Sak oil displacement with enriched gas studied in this research showed a displacement efficiency of 84.29% at 1.0 HCPVI, 90.18% at 1.5 HCPVI, and 91.53% at 2.0 HCPVI at 53%-C_1 dilution. With this C_1 dilution, the three-phase displacement was locally efficient and fast enough to exhibit a high oil recovery.
- Mass conservation was analyzed for multiphase transitions in 1D oil displacement. Results showed that redistribution of components on a phase transition between N_P^U and N_P^D phases must occur through an intersection of the N_P^U-phase tie-simplex extension and the N_P^D-phase tie-simplex extension. N_P^U and N_P^D are the numbers of phases upstream and downstream of the phase transition, respectively.

Nomenclature

c_{ij} = volumetric fraction of component i in phase j
$\underline{c}_j$ = vector consisting of c_{ij} as defined in Eq. B-4
C_i = overall volume fraction of component i
f_j = fractional flow of phase j
F_i = overall fractional flow of component i
L_1 = oleic phase
L_2 = solvent-rich liquid phase
N_j (j=1, 2, or 3) = nonoleic phase (i.e., L_2 or V)
N_C = number of components
N_P = number of phases
P_C = critical pressure
S_j = saturation of phase j
T_C = critical temperature
t_D = dimensionless time in PV
V = gaseous phase
V_C = critical volume
x_D = dimensionless distance from the injector
$\underline{x}_j$ = vector consisting of x_{ij}
x_{ij} = mole fraction of component i in phase j
$\underline{z}^{\text{int}}$ = intersection composition
γ = parameter defined in Eq. B-5
Γ = parameter defined in Eqs. 5 and 6
δ = distance defined in Eqs. 5 and 6
ε = small values used in Eqs. 1, 3, 5, and 6
Λ = dimensionless shock velocity

Superscripts

D = Downstream
U = Upstream

Acknowledgments

This research was partly supported by research grants from the Natural Sciences and Engineering Council of Canada (No. RGPIN 418266) and Japan Petroleum Exploration Company. Ryosuke Okuno was awarded the SPE Petroleum Engineering Junior Faculty Research Initiation Award. Zhongguo Xu has received a scholarship from the China Scholarship Council. We gratefully acknowledge these supports. We also thank Kamy Sepehrnoori for providing the UTCOMP simulator. Flow simulations in this research were conducted by use of the computational facility of Compute Canada.

References

Aghbash, V.N. and Ahmadi, M. 2012. Evaluation of CO_2-EOR and Sequestration in Alaska West Sak Reservoir Using Four-Phase Simulation Model. Presented at the SPE Western Regional Meeting, Bakersfield, California, 21–23 March. SPE-153920-MS. http://dx.doi.org/10.2118/153920-MS.

Ahmadi, K. 2011. *Advances in Calculation of Minimum Miscibility Pressure*. PhD dissertation, the University of Texas at Austin, Austin, Texas (May 2011).

Ahmadi, K. and Johns, R.T. 2011. Multiple-Mixing-Cell Method for MMP Calculations. *SPE J.* **16** (4): 733–742. http://dx.doi.org/10.2118/116823-PA.

Bluma, M. and Deiters, U.K. 1999. A Classification of Phase Diagrams of Ternary Fluid Systems. *Phys. Chem. Chem. Phys.* **1** (18): 4307–4313. http://dx.doi.org/10.1039/A904863D.

Calsep. 2012. PVTsim Version 19.2.0. Lyngby, Denmark: Calsep International Consultants. www.pvtsim.com.

Chang. Y.-B. 1990. *Development and Application of an Equation of State Compositional Simulator*. PhD dissertation, the University of Texas at Austin, Austin, Texas (August 1990).

Chang. Y.-B., Pope, G.A. and Sepehrnoori, K. 1990. A Higher-Order Finite-Difference Compositional Simulator. *J. Pet. Sci. Eng.* **5** (1): 35–50. http://dx.doi.org/10.1016/0920-4105(90)90004-M.

Chang. Y.-B., Lim, M.T., Pope, G.A., and Sepehrnoori, K. 1994. CO_2 Flow Patterns Under Multiphase Flow: Heterogeneous Field-Scale Conditions. *SPE Res Eval & Eng* **9** (3): 208–216. http://dx.doi.org/10.2118/22654-PA.

Creek, J.L. and Sheffield, J.M. 1993. Phase Behavior, Fluid Properties, and Displacement Characteristics of Permian Basin Reservoir Fluid/CO_2 Systems. *SPE Res Eval & Eng* **8** (1): 34–42. http://dx.doi.org/10.2118/20188-PA.

Deiters, U.K. and Pegg, I.L. 1989. Systematic Investigation of the Phase Behavior in Binary Fluid Mixtures. I. Calculations Based on the Redlich-Kwong Equation of State. *J. Chem. Phys.* **90** (11): 6632–6641. http://dx.doi.org/10.1063/1.456280.

Deiters, U. and Schneider, G.M. 1976. Fluid Mixtures at High Pressures. Computer Calculations of the Phase Equilibria and the Critical Phenomena in Fluid Binary Mixtures From the Redlich-Kwong Equation of State. *Berichte der Bunsengesellschaft fuer Physikalische Chemie* **80** (12): 1316–1321. http://dx.doi.org/10.1002/bbpc.19760801215.

DeRuiter, R.A., Nash, L.J. and Singletary, M.S. 1994. Solubility and Displacement Behavior of a Viscous Crude with CO_2 and Hydrocarbon Gases. SPE Res Eval & Eng **9** (2): 101–106. http://dx.doi.org/10.2118/20523-PA.

Dickson, J.L., Clingman, S., Dittaro, L.M., et al. 2011. Design Approach and Early Field Performance for a Solvent-Assisted SAGD Pilot at Cold Lake, Canada. Presented at the SPE Heavy Oil Conference and Exhibition, Kuwait City, Kuwait, 12–14 December. SPE-150639-MS. http://dx.doi.org/10.2118/150639-MS.

Dindoruk, B. 1992. *Analytical Theory of Multiphase, Multicomponent Displacement in Porous Media*. PhD dissertation, Stanford University, Stanford, California (June 1992).

Enick, R., Holder, G.D. and Morsi, B.I. 1985. Critical and Three Phase Behavior in the Carbon Dioxide/Tridecane System. *Fluid Phase Equilibr.* **22** (2): 209–224. http://dx.doi.org/10.1016/0378-3812(85)85020-2.

Galindo, A. and Blas, F.J. 2002. Theoretical Examination of the Global Fluid Phase Behavior and Critical Phenomena in Carbon Dioxide + *n*-Alkane Binary Mixtures. *J. Phys. Chem. B* **106** (17): 4343–4564. http://dx.doi.org/10.1021/jp013402h.

Gardner, J.W., Orr, F.M. Jr. and Patel, P.D. 1981. The Effect of Phase Behavior on CO_2-Flood Displacement Efficiency. *J. Pet. Tech.* **33** (11): 2067–2081. http://dx.doi.org/10.2118/8367-PA.

Gauter, K. 1999. *Fluid Multiphase Behavior in Ternary Systems of Near-Critical CO_2*. PhD dissertation, the Technical University of Berlin, Berlin, Germany (January 1999).

Gauter, K., Heidemann, R.A. and Peters, C.J. 1999. Modeling of Fluid Multiphase Equilibria in Ternary Systems of Carbon Dioxide as the Near-Critical Solvent and Two Low-Volatile Solutes. *Fluid Phase Equilibr.* 158–160 (June): 133–141. http://dx.doi.org/10.1016/S0378-3812(99)00122-3.

Godbole, S.P., Thele, K.J. and Reinbold, E.W. 1995. EOS Modeling and Experimental Observations of Three-Hydrocarbon-Phase Equilibria. *SPE Res Eng* **10** (2): 101–108. http://dx.doi.org/10.2118/24936-PA.

Gregorowicz, J. and de Loos, Th.W. 1996. Modeling of the Three Phase LLV Region for Ternary Hydrocarbon Mixtures With the Soave-Redlich-Kwong Equation of State. *Fluid Phase Equilibr.* **118** (1): 121–132. http://dx.doi.org/10.1016/0378-3812(95)02845-5.

Guler, B., Wang, P., Delshad, M., et al. 2001. Three- and Four- Phase Flow Compositional Simulations of CO_2/NGL EOR. Presented at the SPE Annual Technical Conference and Exhibition, New Orleans, Louisiana, 30 September3 October. SPE-71485-MS. http://dx.doi.org/10.2118/71485-MS.

Gupta, S.C., Gittins, S. and Picherack, P. 2005. Field Implementation of Solvent Aided Process. *J Can Pet Technol* **44** (11): 8–13. http://dx.doi.org/10.2118/05-11-TN1.

Gupta, S.C., and Gittins, S.D. 2006. Christina Lake Solvent Aided Process Pilot. *J Can Pet Technol* **45** (9): 15–18. http://dx.doi.org/10.2118/06-09-TN.

Helfferich, F.G. 1981. Theory of Multicomponent, Multiphase Displacement in Porous Media. *SPE J.* **21** (1): 51–62. http://dx.doi.org/10.2118/8372-PA.

Henry, R.L. and Metcalfe, R.S. 1983. Multiple-Phase Generation During Carbon Dioxide Flooding. *SPE J.* **23** (4): 595–601. http://dx.doi.org/10.2118/8812-PA.

Hornbrook, M.W., Dehghani, K., Qadeer, S., et al. 1991. Effects of CO_2 Addition to Steam on Recovery of West Sak Crude Oil. *SPE Res Eng* **6** (3): 278–286. http://dx.doi.org/10.2118/18753-PA.

Inaganti, M.S. 1994. *Miscible EOR Studies for Schrader Bluff Heavy Oil Reservoir, North Slope of Alaska: Slim Tube Displacement and Fluid Characterization*. MS thesis, University of Alaska Fairbanks, Fairbanks, Alaska.

Jessen, K., Stenby, E.H. and Orr, F.M. Jr. 2004. Interplay of Phase Behavior and Numerical Dispersion in Finite-Difference Compositional Simulation. *SPE J.* **9** (2): 193–201. http://dx.doi.org/10.2118/75134-MS.

Johns, R.T. 1992. *Analytical Theory of Multicomponent Gas Drives with Two-Phase Mass Transfer*. PhD dissertation, Stanford University, Stanford, California (May 1992).

Johns, R.T. and Orr, F.M. Jr. 1996. Miscible Gas Displacement of Multicomponent Oils. *SPE J.* **1** (1): 39–50. http://dx.doi.org/10.2118/30798-PA.

Johns, R.T., Sah, P., and Sabramanian, S.K. 2000. Effect of Gas Enrichment Above the MME on Oil Recovery in Enriched-Gas Floods. *SPE J.* **5** (3): 331–338. http://dx.doi.org/10.2118/65704-PA.

Johns, R.T., Yuan, H. and Dindoruk, B. 2004. Quantification of Displacement Mechanisms in Multicomponent Gasfloods. *SPE J.* **9** (3): 314–321. http://dx.doi.org/10.2118/88999-PA.

Khan, S.A., Pope, G.A. and Sepehrnoori, K. 1992. Fluid Characterization of Three-Phase CO_2/Oil Mixtures. Presented at the SPE/DOE Enhanced Oil Recovery Symposium, Tulsa, Oklahoma, 22–24 April. SPE-24130-MS. http://dx.doi.org/10.2118/24130-MS.

Khataniar, S., Kamath, V.A., Patil, S.L., et al. 1999. CO_2 and Miscible Gas Injection for Enhanced Recovery of Schrader Bluff Heavy Oil. Presented at the SPE International Thermal Operations/Heavy Oil Symposium, Bakersfield, California, 17–19 March. SPE-54085-MS. http://dx.doi.org/10.2118/54085-MS.

Kohn, J.P., Kim, Y.J. and Pan, Y.C. 1966. Partial Miscibility Phenomena in Binary Hydrocarbon Systems Involving Ethane. *J. Chem. Eng. Data* **11** (3): 333–335. http://dx.doi.org/10.1021/je60030a012.

LaForce, T.C. 2005. *Mathematics of Partially Miscible Three-Phase Flow*. PhD dissertation, the University of Texas at Austin, Austin, Texas (May 2005).

LaForce, T.C. 2012. Insight From Analytical Solutions for Improved Simulation of Miscible WAG Flooding in One Dimension. *Computat. Geosci.* **16** (4): 1007–1020. http://dx.doi.org/10.1007/s10596-012-9300-8.

LaForce, T.C., Jessen, K. and Orr, F.M. Jr. 2008a. Four-Component Gas/Water/Oil Displacements in One Dimension: Part I. Structure of the Conservation Law. *Transport Porous Med.* **71** (2): 199–216. http://dx.doi.org/10.1007/s11242-008-9311-z.

LaForce, T.C., Jessen, K. and Orr, F.M. Jr. 2008b. Four-Component Gas/Water/Oil Displacements in One Dimension: Part II. Example Solutions. *Transport in Porous Media* **72** (1): 83–96. http://dx.doi.org/10.1007/s11242-007-9137-0.

LaForce, T.C. and Johns, R.T. 2005a. Analytical Solutions for Surfactant-Enhanced Remediation of Nonaqueous Phase Liquids. *Water Resour. Res.* **41** (10): 1–14. http://dx.doi.org/10.1029/2004WR003862.

LaForce, T.C. and Johns, R.T. 2005b. Composition Routes for Three-Phase Partially Miscible Flow in Ternary Systems. *SPE J.* **10** (2): 161–174. http://dx.doi.org/10.2118/89438-PA.

LaForce, T. and Johns, R.T. 2010. Effect of initial gas saturation on miscible gasflood recovery. *Journal of Petroleum Science and Engineering* **70** (3–4): 198–203. http://dx.doi.org/10.1016/j.petrol.2009.11.011.

LaForce, T.C. and Orr, F.M. Jr. 2009. Four-Component Gas/Water/Oil Displacements in One Dimension: Part III. Development of Miscibility. *Transport Porous Med.* **79** (2): 225–247. http://dx.doi.org/10.1007/s11242-008-9311-z.

LaForce, T.C. and Orr, F.M. Jr. 2008. Development of Gas/Oil Miscibility in Water and Gas Injection. Presented at the SPE Annual Technical Conference and Exhibition, Denver, Colorado, 21–24 September. SPE-116119-MS. http://dx.doi.org/10.2118/116119-MS.

Lake, L.W. 1989. *Enhanced Oil Recovery*. Upper Saddle River, New Jersey: Prentice-Hall, Inc.

Li, D., Kumar, K. and Mohanty, K.K. 2003. Compositional Simulation of WAG Process for a Viscous Oil. Presented at the SPE Annual Technical Conference and Exhibition, Denver, Colorado, 5–8 October. SPE-84074-MS. http://dx.doi.org/10.2118/84074-MS.

Lohrenz, J., Bray, B.C. and Clark, C.R. 1964. Calculating Viscosities of Reservoir Fluids from Their Compositions. *J Pet Technol* **16** (10): 1171–1176. http://dx.doi.org/10.2118/915-PA.

Madarapu, R.R., Khataniar, S. and Dandekar, A.Y., 2002. A Simulation Study of Enhanced Recovery of Schrader Bluff Heavy Oil by Immiscible and Miscible Gas Injection. Presented at the SPE Western Regional/AAPG Pacific Section Joint Meeting, Anchorage, Alaska, 20–22 May. SPE-76776-MS. http://dx.doi.org/10.2118/76776-MS.

Malik, Q.M. and Islam, M.R. 2000. CO_2 Injection in the Weyburn Field of Canada: Optimization of Enhanced Oil Recovery and Greenhouse Gas Storage with Horizontal Wells. Presented at the SPE/DOE Improved Oil Recovery Symposium, Tulsa, Oklahoma, 3–5 April. SPE-59327-MS. http://dx.doi.org/10.2118/59327-MS.

Mallison, B.T., Gerritsen, M.G., Jessen, K., et al. 2005. High Order Upwind Schemes for Two-Phase, Multicomponent Flow. *SPE J.* **10** (3): 297–311. http://dx.doi.org/10.2118/79691-PA.

McGuire, P.L., Redman, R.S., Jhaveri, B.S., et al. 2005. Viscosity Reduction WAG: An Effective EOR Process for North Slope Viscous Oils. Presented at the SPE Western Regional Meeting, Irvine, California, 30 March–1 April. SPE-93914-MS. http://dx.doi.org/10.2118/93914-MS.

McGuire, P.L., Spence, A.P. and Redman, R.S. 2001. Performance Evaluation of a Mature Miscible Gasflood at Prudhoe Bay. *SPE Res Eval & Eng* **4** (4): 318–326. http://dx.doi.org/10.2118/72466-PA.

McKean, T.A.M., Thomas, A.H., Chesher, J.R., et al. 1999. Schrader Bluff CO_2 EOR Evaluation. Presented at the SPE Western Regional Meeting, Anchorage, Alaska, 26–27 May. SPE-54619-MS. http://dx.doi.org/10.2118/54619-MS.

Mizenko, G.J. 1992. North Cross (Devonian) Unit CO_2 Flood: Status Report. Presented at the SPE/DOE Enhanced Oil Recovery Symposium, Tulsa, Oklahoma, 22–24 April. SPE-24210-MS. http://dx.doi.org/10.2118/24210-MS.

Mohanty, K.K., Masino, W.H. Jr., Ma, T.D., et al. 1995. Role of Three-Hydrocarbon-Phase Flow in a Gas-Displacement Process. *SPE Res Eng* **10** (3): 214–221. http://dx.doi.org/10.2118/24115-PA.

Mushrif, S.H. 2004. *Determining Equation of State Binary Interaction Parameters Using K- and L-Points*. MS thesis, the University of Saskatchewan, Saskatoon, Canada (October 2004).

Mushrif, S.H. and Phoenix, A.V. 2008. Effect of Peng-Robinson Binary Interaction Parameters on the Predicted Multiphase Behavior of Selected Binary Systems. *Ind. Eng. Chem. Res.* **47** (16): 6280–6288. http://dx.doi.org/10.1021/ie800599t.

Ogino, K. 1988. *Compositional Simulation of Carbon Dioxide Oil Recovery Experiments*. MS thesis, the University of Texas at Austin, Austin, Texas.

Okuno, R. 2009. *Modeling of Multiphase Behavior for Gas Flooding Simulation*. PhD dissertation, the University of Texas at Austin, Austin, Texas (August 2009).

Okuno, R., Johns, R.T. and Sepehrnoori, K. 2011. Mechanisms for High Displacement Efficiency of Low-Temperature CO_2 Floods. *SPE J.* **16** (4): 751–767. http://dx.doi.org/10.2118/129846-PA.

Okuyiga, M.O. 1992. Equation of State Characterization and Miscibility Development in a Multiple Phase Hydrocarbon System. Presented at the SPE Annual Technical Conference and Exhibition, Washington, DC, 4–7 October. SPE-24937-MS. http://dx.doi.org/10.2118/24937-MS.

Orr, F.M., Jr. 2007. *Theory of Gas Injection Processes*. Holte, Denmark: Tie-Line Publications.

Patel, P.D., Christman, R.G. and Gardner, J.W. 1987. An Investigation of Unexpectedly Low Field-Observed Fluid Mobilities During Some CO_2 Tertiary Floods. *SPE Res Eng* **2** (4): 507–513. http://dx.doi.org/10.2118/14308-PA.

Peng, D.-Y. and Robinson, D.B. 1976. A New Two-Constant Equation of State. *Ind. Eng. Chem. Fundamen.* **15** (1): 59–64. http://dx.doi.org/10.1021/i160057a011.

Peters, C.J. 1994. Multiphase Equilibria in Near-Critical Solvents. In *Supercritical Fluids*, ed. E. Kiran and J.M.H. Levelt Sengers, 117–145. Dordrecht, The Netherlands: Springer Netherlands. http://dx.doi.org/10.1007/978-94-015-8295-7_5.

Polishuk, I., Wisniak, J. and Segura, H., 2004. Estimation of Liquid-Liquid-Vapor Equilibria in Binary Mixtures of n-Alkanes. *Ind. Eng. Chem. Res.* **43** (18): 5957–5964. http://dx.doi.org/10.1021/ie049797j.

Pontious, S.B. and Tham, M.J. 1978. North Cross (Devonian) Unit CO_2 Flood-Review of Flood Performance and Numerical Simulation Model. *J. Pet. Tech.* **30** (12): 1706–1714. http://dx.doi.org/10.2118/6390-PA.

Reid, T. 1994. Study of Hydrocarbon Miscible Solvent Slug Injection Process for Improved Recovery of Heavy Oil From Schrader Bluff Pool, Milne Point Unit, Alaska. Annual Report for DE-FG22-93BC14864 for the US Department of Energy. Petroleum Development Laboratory, University of Alaska Fairbanks, Fairbanks, Alaska (1 January–31 March 1993).

Rogers, J.D. and Grigg, R.B. 2001. A Literature Analysis of the WAG Injectivity Abnormalities in the CO_2 Process. *SPE Res Eval & Eng* **4** (5): 375–386. http://dx.doi.org/10.2118/73830-PA.

Roper, M. 1989. *An Experimental Study of CO_2/West-Sak-Crude-Oil Phase Behavior*. MS thesis, University of Alaska Fairbanks, Alaska, Fairbanks, Alaska.

Rowlinson, J.S. 1959. *Liquids and Liquid Mixtures*. London, UK: Butterworths Publications Ltd.

Rowlinson, J.S. and Freeman, P.I. 1961. Lower Critical Solution Points in Hydrocarbon Mixtures. *Pure Appl. Chem.* **2** (1–2): 329–334. http://dx.doi.org/10.1351/pac196102010329.

Scott, R.L. and van Konynenburg, P.H. 1970. Static Properties of Solutions. van der Waals and Related Models for Hydrocarbon Mixtures. *Discuss. Faraday Soc.* **49**: 87–97. http://dx.doi.org/10.1039/DF9704900087.

Sharma, A.K., Patil, S.L., Kamath, V.A., et al. 1989. Miscible Displacement of Heavy West Sak Crude by Solvents in Slim Tube. Paper SPE 18761 presented at the SPE California Regional Meeting, Bakersfield, California, 5–7 April. http://dx.doi.org/10.2118/18761-MS.

Shu, W.R. and Hartman, K.J. 1988. Effect of Solvent on Steam Recovery of Heavy Oil. *SPE Res Eng* **3** (2): 457–465. http://dx.doi.org/10.2118/14223-PA.

Sohrabi, M., Jamiolahmady, M. and Al-Quraini, A. 2007. Heavy Oil Recovery by Liquid CO_2/Water Injection. Presented at the EUROPEC/EAGE Conference and Exhibition, London, AQ11 UK, 1114 June. SPE-107163-MS. http://dx.doi.org/10.2118/107163-MS.

Solano, R., Johns, R.T. and Lake, L.W. 2001. Impact of Reservoir Mixing on Recovery in Enriched-Gas Drives Above the Minimum Miscibility Enrichment. *SPE Res Eval & Eng* **4** (5): 358–365. http://dx.doi.org/10.2118/73829-PA.

Stein, M.H., Frey, D.D., Walker, R.D., et al. 1992. Slaughter Estate Unit CO_2 Flood: Comparison Between Pilot and Field-Scale Performance. *J Pet Technol* **44** (9): 1026–1032. http://dx.doi.org/10.2118/19375-PA.

Taber, J.J., Martin, F.D. and Seright, R.D. 1997. EOR Screening Criteria Revisited - Part 1: Introduction to Screening Criteria and Enhanced Recovery Field Projects. *SPE Res Eng* **12** (3): 189–198. http://dx.doi.org/10.2118/35385-PA.

Tanner, C.S., Baxley, P.T., Crump III, J.G., et al. 1992. Production Performance of the Wasson Denver Unit CO_2 Flood. Presented at the SPE/DOE Enhanced Oil Recovery Symposium, Tulsa, Oklahoma, 22–24 April. SPE-24156-MS. http://dx.doi.org/10.2118/24156-MS.

Targac, G.W., Reman, R.S., Davis, E.R., et al. 2005. Unlocking the Value in West Sak Heavy Oil. Presented at SPE International Thermal Operations and Heavy Oil Symposium, Calgary, Alberta, Canada, 13 November. SPE-97856-MS. http://dx.doi.org/10.2118/97856-MS.

Tchelepi, H.A. and Orr, F.M. Jr. 1994. Interaction of Viscous Fingering, Permeability Heterogeneity and Gravity Segregation in Three Dimensions. *SPE Res Eng* **9** (4): 266–271. http://dx.doi.org/10.2118/25235-PA.

Uzunov, D.I. 1993. *Introduction to the Theory of Critical Phenomena*. Singapore: World Scientific Publishing.

van Konynenburg, P.H. 1968. *Critical Lines and Phase Equilibria in Binary Mixtures*. PhD dissertation, University of California, Los Angeles, California.

van Konynenburg, P.H. and Scott, R.L. 1980. Critical Lines and Phase Equilibria in Binary van der Waals Mixtures. *Phil. Trans. R. Soc. Lond. A* **298** (1442): 495–540. http://dx.doi.org/10.1098/rsta.1980.0266.

van Odyck, D.E.A., Lovett, S., Monmont, F., et al. 2012. An Efficient Shock Capturing Scheme for Multicomponent Multiphase Thermal Flow in Porous Media. *P. Roy. Soc. Lond. A Mat.* **468** (2147): 3413–3440. http://dx.doi.org/10.1098/rspa.2012.0152.

Varotsis, N., Stewart, G., Todd, A.C., et al. 1986. Phase Behavior of Systems Comprising North Sea Reservoir Fluids and Injection Gases. *J Pet Technol* **38** (11): 1221–1233. http://dx.doi.org/10.2118/12647-PA.

Wang, Y., Lin, C.-Y., Bidinger, C., et al. 2003. Compositional Modeling of Gas Injection With Three Hydrocarbon Phases for Schrader Bluff EOR. Presented at the SPE Annual Technical Conference and Exhibition, Denver, Colorado, 5–8 October. SPE-84180-MS. http://dx.doi.org/10.2118/84180-MS.

Wang, X. and Strycker, A. 2000. Evaluation of CO_2 Injection with Three Hydrocarbon Phases. Presented at the International Oil and Gas Conference and Exhibition in China, Beijing, China, 7–10 November. SPE-64723-MS. http://dx.doi.org/10.2118/64723-MS.

Xu, Z. 2012. *Displacement Efficiency of Solvent Floods with Three Partially Miscible Phases*. MEng project report, the University of Alberta, Edmonton, Alberta (June 2012).

Yang, Q. 2006. *Automatic Development of Global Phase Diagrams for Binary Systems in Pressure-Temperature Space*. MS thesis, the University of Saskatchewan, Saskatoon, Canada (August 2006).

Appendix A—Schematic of a Three-Phase Region Bounded by CEP Tie-Lines

A three-phase region has one degree of freedom at a given temperature and pressure for four components. Therefore, a three-phase region is a volumetric region in a quaternary diagram. The three-phase region consists of an infinite number of tie triangles. A tie triangle changes its shape and size within the three-phase region. Two tie triangles are shown to illustrate tie triangles exhibiting near-CEP behavior. A CEP is not a point in composition space, but is a tie-line where two of the three phases are critical in the presence of the other noncritical phase. More details on three-hydrocarbon-phase behavior are given in Okuno (2009).

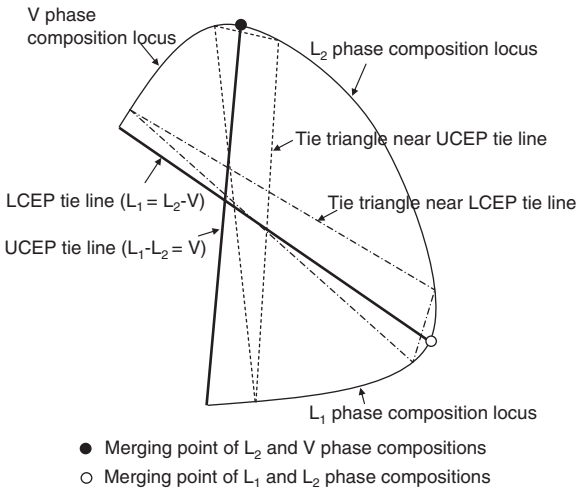

Fig. A-1—Schematic of a three-phase region bounded by CEP tie-lines for a quaternary system at a fixed temperature and pressure.

Appendix B—Mass Conservation on Multiphase Transitions

Conservation of mass for a component in N_P-phase flow through porous media is considered with the following assumptions:

- 1D flow with no gravity
- Constant temperature
- Change in pressure is small over the displacement length
- Constant porosity with time
- No diffusion/dispersion
- No chemical reaction or sorption on the solid phase
- No capillary pressure
- Local equilibrium
- Ideal mixing
- Laminar flow

We then obtain

$$\frac{\partial C_i}{\partial t_D}+\frac{\partial F_i}{\partial x_D}=0, \quad \ldots\ldots\ldots\ldots\ldots\ldots\ldots \text{(B-1)}$$

where t_D is a dimensionless time measured in PV, x_D is a dimensionless distance from the injector, C_i is the overall volume fraction of component i, F_i is the overall fractional flow of component i, and $i=1, 2,\ldots, (N_C-1)$. C_i and F_i are given as

$$C_i=\sum\nolimits_{j=1}^{N_P} S_j c_{ij}$$

$$F_i=\sum\nolimits_{j=1}^{N_P} f_j c_{ij},$$

where S_j is the saturation of phase j, f_j is the fractional flow of phase j, and c_{ij} is the volume fraction of component i in phase j. A detailed derivation of Eq. B-1 is given in Orr (2007).

The weak form of Eq. B-1 is

$$\frac{\mathrm{d}}{\mathrm{d}t_D}\int C_i \mathrm{d}V+\int n\cdot F_i \mathrm{d}S=0, \quad \ldots\ldots\ldots\ldots\ldots \text{(B-2)}$$

where V and S are the volume and surface area of the control volume of interest, respectively. n is the outward normal unit vector on surface S. Let us consider two consecutive gridblocks in a 1D simulation model, where N_P^U and N_P^D phases are present in the upstream and downstream cells, respectively, at a given time. A uniform grid size of Δx_D is considered.

Suppose a phase transition between N_P^U and N_P^D propagates at a dimensionless velocity of $v_D=\Delta x_D/\Delta t_D$, where Δt_D is a certain time period in PV. Discretization of Eq. B-2 with Δx_D and Δt_D using the one-point upstream weighting for the flux term yields

$$v_D=\frac{\Delta x_D}{\Delta t_D}=\frac{F_i^U-F_i^D}{C_i^U-C_i^D}. \quad \ldots\ldots\ldots\ldots\ldots\ldots \text{(B-3)}$$

Rearrangement of Eq. B-3 gives

$$\sum\nolimits_{j=1}^{N_P^U}\left(v_D S_j^U-f_j^U\right)\underline{c}_j^U=\sum\nolimits_{j=1}^{N_P^D}\left(v_D S_j^D-f_j^D\right)\underline{c}_j^D, \quad \ldots\ldots \text{(B-4)}$$

where $\underline{c}_j$ is a vector consisting of c_{ij}. Dividing Eq. B-4 by (v_D-1),

$$\sum\nolimits_{j=1}^{N_P^U}\gamma_j^U\underline{c}_j^U=\sum\nolimits_{j=1}^{N_P^D}\gamma_j^D\underline{c}_j^D, \quad \ldots\ldots\ldots\ldots\ldots \text{(B-5)}$$

where $\gamma_j^U=\dfrac{v_D S_j^U-f_j^U}{v_D-1}$ and $\gamma_j^D=\dfrac{v_D S_j^D-f_j^D}{v_D-1}$. Note that $\sum_{j=1}^{N_P^U}\gamma_j^U=1.0$ and $\sum_{j=1}^{N_P^D}\gamma_j^D=1.0$.

Components are redistributed on a multiphase transition. Eq. B-5 indicates that the redistribution of components must occur through an intersection of the N_P^U-phase tie-simplex extension and the N_P^D-phase tie-simplex extension for the phase transition between the N_P^U and N_P^D phases. For example, a phase transition between two and three phases must occur through an intersection of the tie-line extension and the tie-triangle extension in composition space, as shown in Figs. 30 and 31.

A special case of multiphase transitions is a phase-transition shock in the MOC solution of Eq. B-1. The conservation equations for a shock are called the jump conditions. The jump conditions for a shock with a dimensionless velocity of Λ are

$$\Lambda = \frac{F_i^U - F_i^D}{C_i^U - C_i^D}, \quad \ldots\ldots\ldots\ldots\ldots\ldots\ldots\ldots \text{(B-6)}$$

where $i = 1, 2, \ldots, (N_C - 1)$. Replacement of v_D in Eqs. B-4 and B-5 with Λ results in

$$\sum_{j=1}^{N_P^U} \gamma_j^U \underline{c}_j^U = \sum_{j=1}^{N_P^D} \gamma_j^D \underline{c}_j^D, \quad \ldots\ldots\ldots\ldots\ldots\ldots \text{(B-7)}$$

where $\gamma_j^U = \dfrac{\Lambda S_j^U - f_j^U}{\Lambda - 1}$ and $\gamma_j^D = \dfrac{\Lambda S_j^D - f_j^D}{\Lambda - 1}$. Note that $\sum_{j=1}^{N_P^U} \gamma_j^U = 1.0$ and $\sum_{j=1}^{N_P^D} \gamma_j^D = 1.0$.

Eq. B-7 indicates that a shock must occur through an intersection of the tie-simplex extension of $(N_P^D - 1)$ dimensions and that of $(N_P^U - 1)$ dimensions. For $(N_P^D, N_P^U) = (1, 2)$, the previous result reduces to the well-known result of Helfferich (1981), that a shock between one and two phases must occur on the tie-line extension. For $(N_P^D, N_P^U) = (2, 3)$, a shock between two and three phases must occur through an intersection of the tie-triangle-extension plane and the tie-line extension. Eq. B-5 is of the identical form with the generalized jump conditions on multiphase transition presented in Eq. B-7. The difference is that v_D in Eq. B-5 is in general not the same as the shock velocity Λ in Eq. B-7. Eq. B-5 is even more general, and applicable in mechanistic interpretation of mass transfer on a multiphase transition in the presence of numerical dispersion.

LaForce (2005) and LaForce and Johns (2005a, b) studied three-phase displacement of oil with three components. In their studies, composition paths are constrained to exist in composition space of two dimensions. A tie triangle and tie-lines are always on the 2D composition plane in their cases. The proof given here was neither needed nor presented in their research.

SI Metric Conversion Factors

ft	× 3.048*	E−01 = m
°F	(°F–32)/1.8	= °C
psi	× 6.894757	E+00 = kPa

*Conversion factor is exact.

Ryosuke Okuno has served as an assistant professor of petroleum engineering in the Department of Civil & Environmental Engineering at the University of Alberta since 2010. His research and teaching interests include EOR, thermal oil recovery, oil displacement theory, numerical reservoir simulation, thermodynamics, multiphase behavior, and applied mathematics. Okuno has 7 years of industrial experience as a reservoir engineer with Japan Petroleum Exploration Company and is a registered professional engineer in Alberta, Canada. He holds bachelor's and master's degrees in geosystem engineering from the University of Tokyo, and a PhD degree in petroleum engineering from the University of Texas at Austin.

Zhongguo Xu is a PhD degree candidate in petroleum engineering in the Department of Civil & Environmental Engineering at the University of Alberta. His research interests include numerical reservoir simulation and multiphase behavior. Xu holds a bachelor's degree from the China University of Petroleum (Beijing) and a master's degree from the University of Alberta, both in petroleum engineering.